

**Design and Characterization of a New Pulsed
Molecular-Beam Valve**

by

Ian Collett

A thesis submitted to the
Faculty of the Undergraduate School of the
University of Colorado in partial fulfillment
of the requirements for the degree of
Bachelor of Science
Department of Physics

2016

This thesis entitled:
Design and Characterization of a New Pulsed Molecular-Beam Valve
written by Ian Collett
has been approved for the Department of Physics

Prof. Heather Lewandowski, Physics

Prof. James Nagle, Physics

Prof. Adam Norris, Applied Math

Date _____

The final copy of this thesis has been examined by the signatories, and we find that both the content and the form meet acceptable presentation standards of scholarly work in the above mentioned discipline.

Collett, Ian (B.S., Engineering Physics)

Design and Characterization of a New Pulsed Molecular-Beam Valve

Thesis directed by Prof. Heather Lewandowski, Physics

A common technique for producing samples of cold molecules that can be trapped and studied is electromagnetic deceleration of a fast moving, but internally cold, supersonic beam. The quality of these samples, which are ideally as cold and dense as possible, is fundamentally limited by the quality of the beam coupled to the decelerator. This thesis outlines the design, construction, and characterization of a new pulsed valve that produces samples of molecules as short as fifty microseconds.

Acknowledgements

First and foremost, thank you to my thesis advisor Professor Heather Lewandowski for providing me with the opportunity to do research in an institute as prestigious as JILA. My years in JILA truly have defined my college career.

Thank you to my fellow group members in the Lewandowski lab: post-doc Philipp Schmid; graduate students Noah Fitch, Travis Briles, Maya Fabrikant, Yomay Shyur, John Gray, and James Greenberg; and undergraduate Kevin Loeffler. Travis served as my mentor on the valve project until his graduation, at which point Yomay took over the position. They were both always eager to help me however possible and answer a multitude of questions.

I would also like to thank the talented JILA staff in the electronics shop and the machine shop. Particularly, I'd like to mention Kim Hagen, who machined the valve flange, and Hans Green, who helped with nearly every tricky aspect of the machining process.

I appreciate the efforts of my thesis defense committee. In addition to Professor Lewandowski, Professors Jamie Nagle and Adam Norris served on the committee. Professor Nagle also (along with Professor John Cumalat) led the honors seminar, providing valuable feedback during my practice talks and, thankfully, tolerating my attempts at humor.

Of course, thank you to my parents, Jeff and Julie, for supporting me (emotionally and financially) throughout my years as an undergraduate. Thank you to Alex for taking the time to read through this thesis at the last minute. And, last but not least, thank you to Elizabeth for her unwavering support in every aspect of my life.

Contents

Chapter	
1	Introduction 1
1.1	Experimental Apparatus 2
1.1.1	Supersonic Expansion 3
1.1.2	Deceleration and Trapping 5
1.1.3	Detection 7
1.2	Pulsed Valves 9
2	Electronic Design and Construction 11
2.1	Design 11
2.1.1	Charge Circuit 11
2.1.2	Discharge Circuit 14
2.1.3	Safety Measures 16
2.2	Construction 17
3	Mechanical Design and Construction 21
3.1	Design 21
3.1.1	Valve Flange 22
3.1.2	Valve Body 24
3.2	Construction 26
3.2.1	Valve Flange 26

3.2.2	Valve Body	28
3.2.3	Full Assembly	41
4	Methods of Valve Characterization	44
4.1	Mechanical Motion	44
4.2	Gas Pulse	49
5	Data and Analysis	54
5.1	Mechanical Motion Results	54
5.2	Gas Pulse Results	59
5.3	Conclusions and Future Work	62
	Bibliography	64

Tables

Table

3.1	Fasteners used in valve assembly	42
-----	--	----

Figures

Figure

1.1	Experimental apparatus	2
1.2	3-D potential well	6
1.3	REMPI of ammonia	8
2.1	Circuit diagram of the valve electronics	12
2.2	Measurement of the peak current	15
2.3	Custom valve electronics	17
2.4	Full circuit diagram	20
3.1	Render of the valve flange	22
3.2	Attachment of the valve housing	23
3.3	Render of the valve body	24
3.4	Valve flange drawing	27
3.5	Base drawing	30
3.6	Electrode drawing	32
3.7	Strip clamps	34
3.8	Strip dimensions before bending	35
3.9	Strip drying rack	36
3.10	Strip bending jig	37
3.11	Finished strips	38

3.12 Magnet yoke	39
3.13 Magnet bracket	40
3.14 Views of the assembled valve body	43
3.15 Views of the valve flange	43
4.1 Early valve prototype	45
4.2 Razor blade measurement of the HeNe intensity profile	48
4.3 Testing chamber	50
5.1 Comparison of Al 6061 and BeCu strips	57
5.2 Comparison of Al 6061 and Al 4043 strips	58
5.3 Effect of pulse length on opening displacement and time	60
5.4 Gas pulse produced by the valve	61

Chapter 1

Introduction

A pulsed valve has a single crucial task in a molecular beam experiment: to control the flow of molecules from a gas reservoir into a vacuum chamber containing the further stages of the experimental apparatus. Before the advent of the pulsed valve nearly forty years ago, such experiments used a continuous beam source [7]. In this case, molecules leak continuously into the vacuum chamber, necessitating large amounts of differential vacuum pumping that is both difficult and expensive to implement. Additionally, continuous beam sources contribute a constant background signal, resulting in less sensitive measurements from the detectors. Now, however, with several decades of improvements in pulsed valve designs, various fields within physics and chemistry have expanded their experimental capabilities.

One such field is that of cold (1 mK to 1 K) and ultracold (<1 mK) molecules [3]. Experimentation with cold and ultracold molecules has increased the understanding of, for example, collisions and reactions in the quantum regime [5]. These experiments require a source of internally cold and dense molecular beams. In this respect, the pulsed valve has certainly left its mark—the quality of the molecular beam is directly coupled to the performance of the valve.

This thesis describes the design, construction and characterization of a new pulsed molecular beam valve. The remainder of Chapter 1 provides background on the experimental apparatus used in our lab to study cold molecules and several types of existing pulsed valves. Chapter 2 and Chapter 3 provide details of the electronic and mechanical design of the new valve. (One of the major goals of this thesis is to provide information sufficient for any experimentalist to build their

own pulsed valve similar to the design presented here. Because of this, the valve construction and assembly illustrated in these two chapters is presented in great detail.) Chapter 4 describes the methods used to gauge the performance of the valve. Chapter 5 analyzes the data to characterize the valve performance. The latter half of Chapter 5 draws conclusions and comments on the future work that remains to fully integrate the valve into the full apparatus.

1.1 Experimental Apparatus

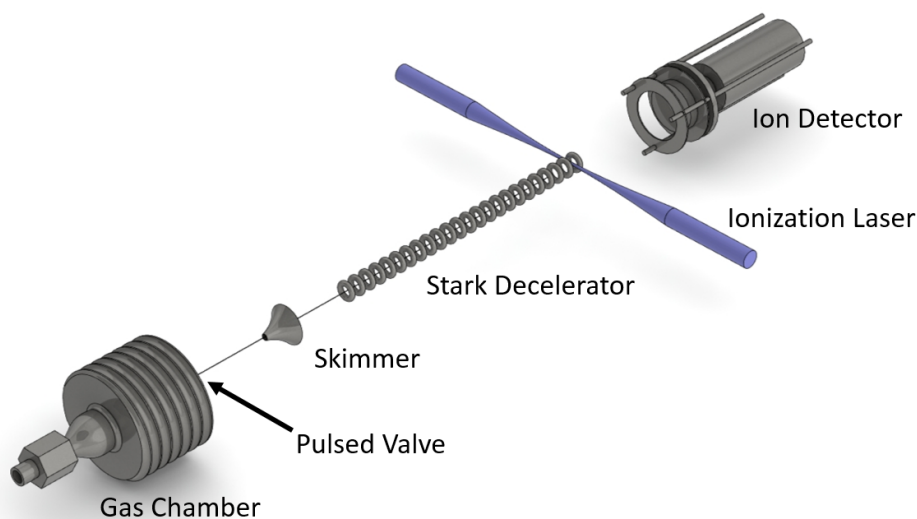


Figure 1.1: A simplified SolidWorks rendering of the entire experimental apparatus. The entire system is held at vacuum pressure (about 10^{-9} Torr).

As previously mentioned, a pulsed valve acts as the interface between a gas reservoir (which contains some sample of gas) and a vacuum chamber (which contains the further stages of the experimental apparatus). When the valve opens, the gas molecules undergo a process called **supersonic expansion**, the result of which is a dense, internally cold molecular beam with a large forward velocity in the lab frame. These types of beams are already suitable for collision experiments.

However, many experiments require longer interaction times. In these cases, the molecules must be decelerated and trapped. Our lab is particularly interested in deceleration of cold molecules

(see the apparatus in Figure 1.1). For neutral molecules with large electric dipole moments, a proven technique to achieve this is **Stark deceleration**, in which time-dependent, inhomogeneous electric fields are used to remove translational kinetic energy from the beam. The slow molecules can then be trapped electrostatically and used in collision studies. To detect the trapped molecules, they are ionized and an electric field is applied to accelerate them towards a microchannel plate detector (MCP).

Although many species can be decelerated, one particular molecule of interest is ammonia (NH_3). An experimental apparatus like the one just described has been used, for example, to decelerate ammonia molecules and co-trap them with cold rubidium atoms to further understand the physics of molecule–atom collisions in the quantum regime [9]. In the following sections, we further describe the three stages of this experimental apparatus (supersonic expansion, deceleration and trapping, and detection) in the context of ammonia.

1.1.1 Supersonic Expansion

In a supersonic expansion, molecules in a high pressure gas reservoir expand through a nozzle into vacuum. In this process, the enthalpy of the molecules in the gas reservoir is converted into translational kinetic energy, resulting in a molecular beam with a high forward velocity in the lab frame that is internally cold (i.e., it has a narrow velocity distribution). In order for supersonic expansion to occur, the mean free path of the molecule must be significantly smaller than the diameter of the nozzle through which the expansion occurs ($\lambda \ll d$). Seeing as the nozzle diameter of a typical pulsed valve is ~ 1 mm and the mean free path of a typical molecule at ambient pressure is ~ 68 nm [10], this condition is certainly upheld (in fact, the pressure in the gas reservoir is held at ~ 850 torr [13]—slightly higher than ambient pressure—so the mean free path of the molecule is even shorter).

In the ideal scenario where all of the enthalpy of the gas is converted into translational kinetic energy, the forward velocity of the beam is [4]

$$v_{max} = \sqrt{\frac{2k_B T_0}{m} \frac{\gamma}{\gamma - 1}}, \quad (1.1)$$

where k_B is Boltzmann's constant, T_0 is the initial temperature in the gas reservoir (usually room temperature), and m is the mass of the atom or molecule. The **adiabatic constant**, γ , is defined as

$$\gamma = \frac{f + 2}{f}, \quad (1.2)$$

where f is the number of degrees of freedom (i.e., translational, rotational, and vibrational). For a monatomic gas, which has only translational degrees of freedom, $\gamma = 5/3$. In the supersonic expansion of krypton at room temperature (294 K), Equation 1.1 yields $v_{max} = 385$ m/s.

For an ideal gas, the supersonic expansion from initial conditions (T_0, P_0) to final conditions (T_1, P_1) has the relation [11]

$$\frac{T_1}{T_0} = \left(\frac{P_1}{P_0}\right)^{(\gamma-1)/\gamma}. \quad (1.3)$$

In other words, a large pressure difference between the gas reservoir and the vacuum chamber results in a colder beam. In our apparatus, the gas reservoir is held at ~ 850 torr, and the first section of the vacuum chamber settles at $\sim 1 \times 10^{-5}$ torr when the valve is operated at a typical repetition rate of 10 Hz. For the supersonic expansion of krypton at room temperature, this equation yields $T_1 = 0.2$ K.

The purpose of using krypton is further means to an end—the krypton acts as a carrier gas to aid in the supersonic expansion of ammonia. To achieve the supersonic expansion of ammonia, the krypton is seeded with a small concentration ($\sim 1\%$) of ammonia molecules. The resulting expansion is the weighted average of the two separate supersonic expansions of the ammonia and krypton. Since ammonia is lighter than krypton, this expansion typically results in a molecular beam traveling at ~ 415 m/s with an internal temperature of ~ 0.1 K. The large ratio of krypton to ammonia is necessary to keep the ammonia molecules from clustering together during the expansion.

After the expansion, the molecular beam reaches the skimmer (the cone-shaped piece depicted in Figure 1.1), which allows only molecules traveling on-axis within the size of the aperture to pass through. The result of this entire stage is an internally cold and collimated molecular beam with a diameter of approximately 2 mm.

1.1.2 Deceleration and Trapping

After being collimated by the skimmer, the molecular beam enters the decelerator. A common technique for decelerating neutral, dipolar molecules is Stark deceleration. One version, the “pulsed decelerator,” uses switching DC voltages on numerous pairs of metal rods to slow molecules passing along its axis [2]. Another version, a technique called **traveling-wave Stark deceleration**, applies sinusoidal AC voltages to ring electrodes, creating a three-dimensional potential well that captures the molecules and slows as it propagates along the decelerator axis [14]. Our lab has recently developed and begun testing a traveling-wave stark decelerator [13], described briefly here.

The decelerator consists of 624 deceleration electrodes and eight trap electrodes, equally spaced at 2 mm and with a ring diameter of 4 mm. Sixteen high-voltage amplifier boxes are required in total—eight to control the voltages of the deceleration electrodes, and eight to control the voltages of the trap electrodes. Every eighth deceleration electrode is electrically connected. The voltage applied to the i th electrode is

$$V_i = V_a \sin\left(\frac{2\pi i}{8} - \omega t\right) \quad (1.4)$$

for $i = 0, 1, \dots, 7$, where V_a is the amplitude (12 kV) and ω is the angular frequency ($\omega = 2\pi f$). The net effect of applying these voltages is to create a three-dimensional potential well. The ωt term governs how quickly the potential well propagates along the decelerator axis. To decelerate the molecules captured within the potential well, the frequency of the sine wave is gradually decreased in time:

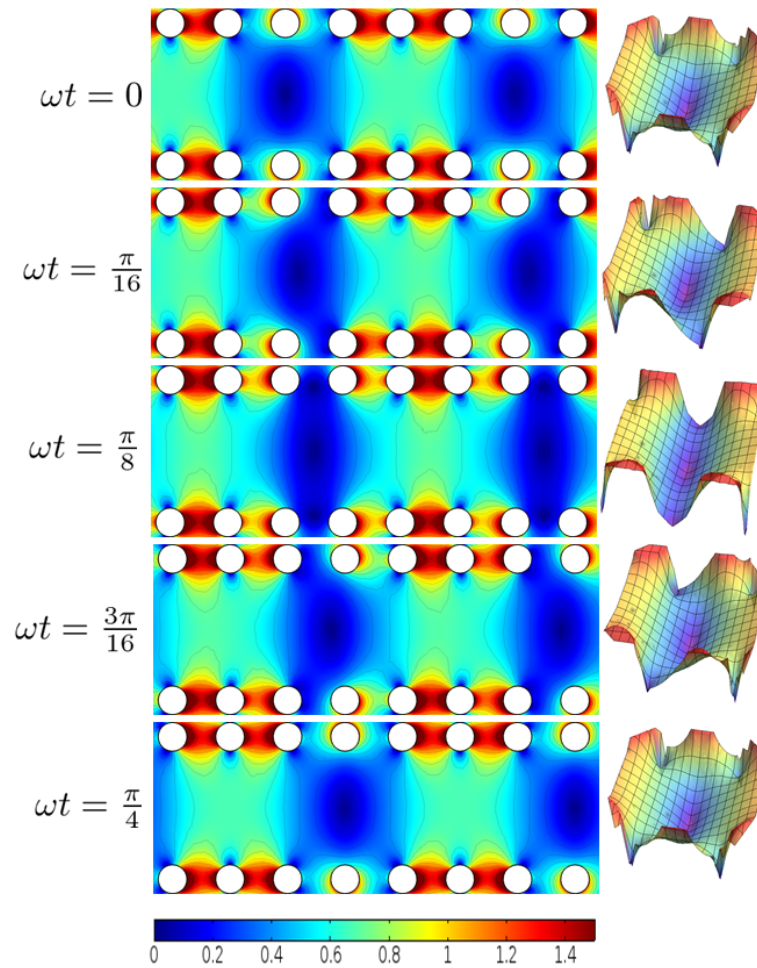


Figure 1.2: A three-dimensional potential well is created by applying time-varying voltages to the electrodes. Every eighth electrode is held at the same voltage (the phase difference between each electrode is $\pi/4$). On the left is a cross-sectional view of the ring electrodes, and on the right is a 3-D view of the potential well formed as it propagates along the center axis of the rings. The color scale shows potential energy in units of Kelvin. Figure from [13].

$$V_i = V_a \sin \left(\frac{\pi i}{8} - 2\pi \left(f_0 t + \frac{\alpha t^2}{2} \right) \right), \quad (1.5)$$

where f_0 is the initial frequency, and α is a negative constant that sets the rate of deceleration. Figure 1.2 shows how the potential well evolves in time.

The final eight rings of the decelerator are the trap rings. Once the potential well has been gradually slowed along the length of the decelerator, the remaining eight high-voltage amplifiers are used to apply DC voltages to the trap rings, creating an electrostatic trap.

The electric fields created by the voltages applied to these rings is at a maximum at the surface of the ring, and at a minimum in the center of the rings where the potential well is located. For this reason, only **weak-field seeking** states of molecules, whose Stark energy decreases with decreasing electric field, can be decelerated using this technique (a molecule in the strong-field seeking state would see a potential hill instead of a potential well). In our specific case, only weak-field seeking states of ammonia are found in the trap at the end of the deceleration phase.

1.1.3 Detection

To detect the ammonia, an ionization technique called **resonance enhanced multi-photon ionization** (REMPI) is used [1]. The REMPI scheme used to detect ammonia is called REMPI 2+1. In this scheme, two photons of 317 nm laser light are used to excite the ammonia to a bound, semi-stable energy level. A third photon is then used to ionize the molecule (see Figure 1.3).

Once the ammonia is ionized, an electric field is applied that accelerates the positively-charged ammonia ions further down the experimental apparatus, towards an MCP. The MCP measures the flux of ions.

REMPI is advantageous because it allows state-selective ionization of molecules (in this case, only one specific quantum state of ammonia is ionized). REMPI also provides spatial resolution of the molecules in the trap. The laser used in REMPI is focused to a small beam waist (about 50 μm) and ionizes only a small volume of the trapped molecules at a time. By running the experiment

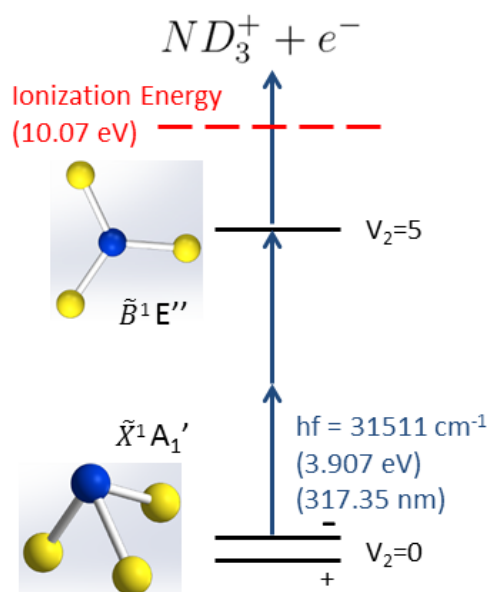


Figure 1.3: Resonance enhanced multi-photon ionization (REMPI) is used to selectively ionize ammonia molecules. Two photons of 317 nm laser light excite the ammonia to a higher bound state, and a third photon ionizes it. Figure from [13].

many times in a row with the ionization laser pointed at a slightly different vertical location in the trap each time, a vertical profile of the number of molecules in the trap can be produced.

1.2 Pulsed Valves

The choice of pulsed valve is an extremely important one when performing a cold molecule experiment. After all, the forces applied by the inhomogeneous electric fields used for Stark deceleration are conservative—no cooling can occur. The cooling (phase space compression) of the molecular beam happens solely during the supersonic expansion. The quality of the supersonic expansion is determined by the performance of the pulsed valve used. For example, a valve that does not open wide enough may not achieve the gas flow required for a true supersonic expansion [17]. This section presents the common types of pulsed valves used to produce molecular beams.

Although high-performance pulsed valves are commercially available, they are generally rather expensive (ten to twenty thousand dollars). The Jordan Valve [16] and the Even-Lavie Valve [6] are two types of commercially available valves. The design of the Jordan Valve consists of two parallel conductors. When a high amount of current flows in opposite directions through the two conductors, a repulsive force separates them slightly, breaking an O-ring seal and opening the valve. On average, the Jordan Valve achieves a gas pulse width of 60 μs FWHM (full-width half-maximum). The Even-Lavie Valve, on the other hand, is a solenoid valve. A current pulsed through a solenoid creates a magnetic field that lifts a metal plunger and opens the valve. The Even-Lavie Valve can achieve an impressive pulse width of 20 μs FWHM.

Another common design of pulsed valve is the piezoelectric transducer (PZT) valve, originally conceived in [15]. Our lab currently uses a PZT valve that produces a gas pulse of 100 μs FWHM. The valve operates on the principle that a disk of piezoelectric material flexes when a high voltage is applied to it. When -1000 V is applied, the disk flexes 100 μm to its full opening displacement [13]. A poppet with an O-ring at its tip is attached to the disk. The seal that the O-ring makes with the valve nozzle is broken, and the gas is allowed to expand into the vacuum chamber.

The design of the valve described in this thesis is based on the design of the Nijmegen Pulsed

Valve (NPV) [19]. The actuator of the NPV is a thin aluminum strip attached on either end to an electrode. The middle of the strip is situated between two permanent neodymium magnets. A small ball is attached to the bottom of the strip and makes a seal with an O-ring mounted on the valve nozzle. When a high current of about 1000 A is sent through the strip via the electrodes, it experiences a Lorentz force that displaces it away from the valve nozzle, opening the valve. With this method, a pulse length as short as 20 μs FWHM can be produced.

The remainder of this thesis describes the design, construction, and testing of a new valve based on the principle of the NPV. The design of the NPV is chosen for a few reasons. First, the design of the NPV is simple enough to be built in house. Second, the NPV has demonstrated the ability to produce a molecular beam pulse with better characteristics than the PZT valve. The goal of the research presented here is to create a reliable pulsed valve that, at the very least, outperforms the PZT valve currently in use in the lab.

Chapter 2

Electronic Design and Construction

This chapter details the custom valve electronics, tasked with producing a short pulse (10 – 50 μs) of high current (at least 1000 A). The electronics are connected to the electrodes of the valve so that the current pulse flows through the metal valve strip. The center of the strip, which lies in between two permanent magnets, feels a Lorentz force upwards when the current flows through it, opening the valve.

2.1 Design

A simplified circuit diagram of the valve electronics is shown in Figure 2.1. The circuitry that drives that valve consists of two coupled RC circuits. In the first RC circuit, the **charge circuit**, a floating power supply in series with a small resistance charges a bank of capacitors with a large capacitance. In the second RC circuit, the **discharge circuit**, the bank of capacitors discharges through the metal valve strip, creating a short duration pulse of high current. The discharge of the capacitor bank through the valve strip is controlled by a MOSFET, which acts as an electronic switch. When a square wave pulse is sent to the gate pin of the MOSFET, it completes the discharging circuit and allows the current to pulse through the valve.

2.1.1 Charge Circuit

In the charge circuit, a floating power supply, adjustable between 0-20 V, charges ten capacitors in parallel (Panasonic EEU-FM1V102) with a total capacitance of 10,000 μF . A small

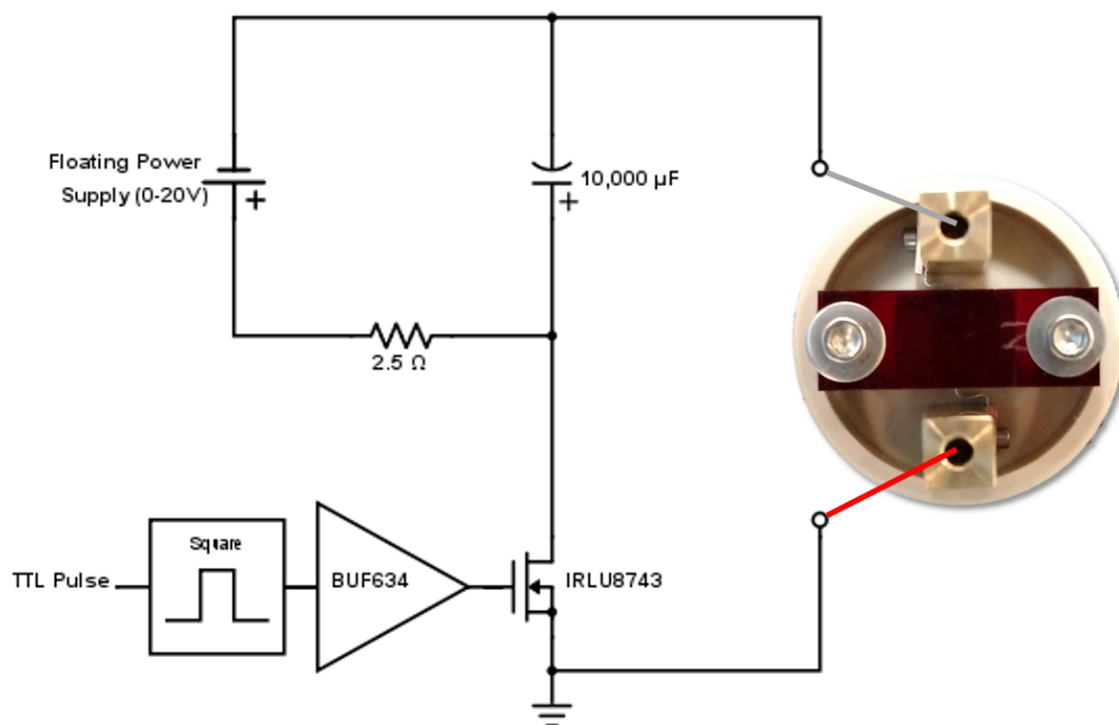


Figure 2.1: A simplified circuit diagram of the valve electronics. Leads from the circuit are attached directly to the valve (shown on the right) via two electrodes.

resistance (2.5Ω) is placed in series with the power supply and the capacitors. Because the valve is designed to operate up to 10 Hz, the capacitors must recharge in a tenth of a second to be ready for the next pulse. The value of the resistance must be small enough to allow the capacitors to fully recharge, and is determined by considering the behavior of this RC circuit. In an RC circuit, the time-dependence of the charge on a capacitor is given by

$$Q(t) = CV \left(1 - e^{-t/\tau} \right), \quad (2.1)$$

where C is the capacitance ($10,000 \mu\text{F}$), V is the voltage across the capacitor plates (the voltage of the floating power supply), and τ is the RC time constant ($\tau = RC$). When $t = \tau$, $Q(\tau) = CV(1 - e^{-1})$. At this point, the capacitors have charged to 63% of their total capacity. When $t = 4\tau$, the capacitors are practically fully charged (98% of total capacity).

If the valve is operating at the maximum rate of 10 Hz, the time between each discharge is approximately 0.1 s. For the capacitors to recharge sufficiently between each current pulse, $\tau \leq 0.025$. Using $\tau = RC$, the resistance needed to achieve this is found to be 2.5Ω .

In choosing this relatively low resistance, another factor must be considered. The time-dependence of the charging current in an RC circuit is given by

$$I(t) = \frac{V}{R} e^{-t/\tau}, \quad (2.2)$$

where $R = 2.5 \Omega$. Consider the case where $V = 20 \text{ V}$, the maximum voltage of the floating power supply. The maximum charging current (at $t = 0$) is given by

$$I_{max} = \frac{V}{R}. \quad (2.3)$$

Equation 2.3 equivalent to Ohm's law. In this case, $I_{max} = 8 \text{ A}$. The power dissipation through the resistor is $P = IV = 160 \text{ W}$. This is certainly more than a standard 1/8 watt resistor can handle! These potentially disastrous effects are mitigated by using four 10Ω , 50 W resistors in parallel.

The equivalent resistance of these four resistors is the required $2.5\ \Omega$, and the 50 W power rating is sufficient to handle the 2 A of current (40 W power dissipation) through each.

Of course, under typical operation, the pulse length is far from long enough to fully discharge the capacitors (see Section 2.1.2). However, choosing this value of resistance ensures that the capacitors will fully recharge in any scenario.

2.1.2 Discharge Circuit

The discharge circuit consists of the bank of capacitors in series with the MOSFET (International Rectifier IRLU8743) and the metal valve strip. Actually, four MOSFETs are used in parallel because the maximum pulsed current rating of each MOSFET is 640 A—less than what is required to effectively operate the valve. Wiring four MOSFETs in parallel allows a peak pulsed current of up to 2560 A. As it turns out, the circuitry achieves a peak current of approximately 1600 A, well within the operating limits of the parallel MOSFETs.

A function generator provides the square wave that drives the pulsed valve. The square wave pulse, at 0 V when low and 5 V when high, has a length of 10-50 μs and a repetition rate of up to 10 Hz. The output of the function generator is connected to the gate pins of the MOSFETs through a buffer (Burr-Brown BUF634). The BUF634 is a high speed, unity-gain, non-inverting amplifier that is in place to prevent the valve electronics from loading the function generator. A second power supply provides the BUF634 with the $\pm 15\ \text{V}$ it requires. When the gate pins of the MOSFETs are at 5 V (i.e., when the square wave pulse is high), the discharge circuit is completed and the current flows through the valve strip.

Unlike the charging circuit, the total resistance of the discharge circuit is not so obvious. Each component contributes a small amount of resistance to the total circuit path. For example, each MOSFET has a drain-to-source resistance of $3.1\ \text{m}\Omega$. Since four are wired in parallel, the total resistance contribution of the MOSFETs is about $0.8\ \text{m}\Omega$. The remainder of the circuit resistance comes from the wires and solder joints connecting the components, as well as from the electrodes and the metal strip on the valve itself. In general, the resistance of a material is

$$R = \frac{\rho L}{A}, \quad (2.4)$$

where L is the length, A is the cross-sectional area, and ρ is the resistivity, an intrinsic property of the material used. In order to produce high current, the resistance of the circuit connections must be as small as possible. This is achieved by choosing circuit connections with low resistivity (copper is the standard choice), short length, and large cross-sectional area (see Section 2.2).

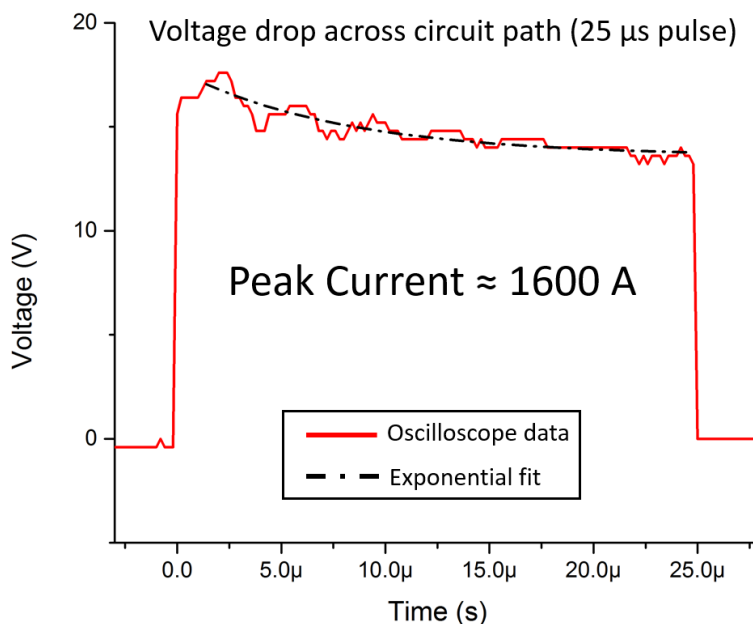


Figure 2.2: The peak current is determined by first measuring the time constant associated with the exponential decay of the voltage drop across the valve strip. After using the time constant to determine the total resistance of the circuit path, the peak current is calculated.

Because the total resistance is so small, it cannot be directly measured by conventional methods. Although it would be possible to theoretically calculate the resistance by considering the resistivities and dimensions of the various parts along the current path, a more reliable method utilizes the RC behavior of the circuit.

The resistance of the circuit can be measured by allowing the current from the charged capacitors to drain through the valve strip. By measuring the voltage drop across the strip and fitting it to an exponential decay function, the time constant can be extracted (see Figure 2.2).

The time constant for the discharging circuit turns out to be $\tau = 1.246 \times 10^{-4}$ s, which yields a total resistance of 12.46 m Ω . When the power supply voltage is set at a maximum of 20 V, the circuit achieves $I_{max} = 1606.4$ A (Equation 2.3).

2.1.3 Safety Measures

With a peak current exceeding 1600 A, one might wonder if any measures are necessary to guarantee safe operation of the valve electronics. However, such high currents are only achieved because of the extremely low resistance of the discharging circuit path. In fact, it is completely safe to touch both of the electrodes of the valve during operation. This scenario can be modeled as two resistors in parallel—the resistance of the human body (usually in excess of 10 k Ω [12]) in parallel with the resistance of the valve strip (no more than a few m Ω). Because of voltage drops associated with other components in the discharge circuit, the voltage drop across the valve strip is less than ten volts, even when using the floating power supply at its maximum voltage of 20 V. The current that flows through each resistor in parallel (a human and the strip) is inversely proportional to the resistance. This means that only about 1 mA of the total 1600 A current would flow through someone touching both of the electrodes (besides, this current pulse only lasts for a few microseconds).

Another concern with such high currents is heating of the valve. After all, assuming that the voltage drop across the strip is 10 V, the power dissipation is $P = IV = 16,000$ W! This huge amount of power is only dissipated for microseconds at a time, however. For example, with a 50 μ s pulse at a 10 Hz repetition rate, the average power is $P_{avg} = 8$ W, which is significantly less than the power dissipation through the resistors in the charging circuit. The fact that the valve has low enough power dissipation to avoid heating up is also important in the context of cold molecule experiments, for obvious reasons.

2.2 Construction

Although the valve electronics consist of common components, the construction of the circuit is less trivial than simply mounting the components on a circuit board. The length and cross-sectional area of the circuit components must be minimized and maximized, respectively, to minimize the total resistance of the circuit. The traces on a standard circuit board have far too small of a cross-sectional area to be appropriate in this application. The solution is to use large gauge wire and copper bars to connect the components along the path of the discharging circuit (the parts of the circuit where the high current does not flow can be constructed using more conventional methods). A photograph of the custom electronics is depicted in Figure 2.3.

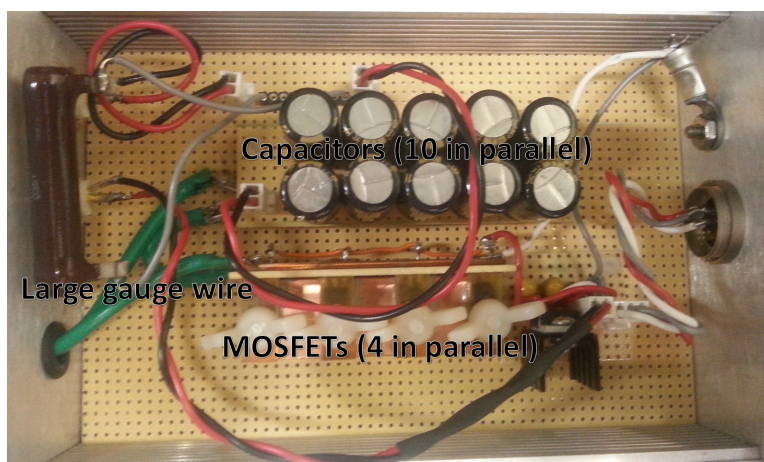


Figure 2.3: A picture of the construction of the valve electronics. Note how the MOSFETs are connected by copper bars, and that large gauge wire (green insulation) is used to make the connections where high current flows.

The electronics are all mounted on a non-plated breadboard (Vector Electronics Vectorbord) inside a small aluminum box. The box contains two electrically isolated BNC inputs, to connect the floating power supply that charges the capacitors and the function generator that provides the square wave pulse, and a DIN connector, to connect the ± 15 V power supply that powers the buffer. The DIN connector, which is not electrically isolated, grounds the aluminum box. The box also contains a small port for the leads that connect to the valve electrodes.

Inside the box, three pins from the DIN connector are used to carry ± 15 V and ground to a small circuit board where they are connected via a three pin Molex connector. On the circuit board, the ± 15 V Molex connections are connected to the power inputs of the BUF634 buffer. A $10 \mu\text{F}$ decoupling capacitor is connected from each power pin on the buffer to ground. The two pins from the function generator BNC connector are connected to this small circuit board through a two pin Molex connector, which then connects the positive voltage input to the input pin of the buffer.

The output pin of the buffer, which carries the square wave pulse, is then connected to the gate pins four MOSFETs in parallel. Small gauge wire is used because no high currents flow on the gate side of the MOSFETs. The packages of the MOSFETs are coated in thermal paste and clamped onto a thick copper bar, which acts as a heat sink. Two-millimeter thick copper sheet cut into thin bars is used to connect the MOSFETs in parallel (one bar is used to connect the source pins, and the other is used to connect the drain pins). The pins of the MOSFETs are soldered directly onto the copper bars with a generous amount of solder. A short section of 14 AWG stranded wire is connected to each the copper bars. The wire connected to the source pin is the lead that connects to the positive valve electrode. The source pin is also grounded through a wire that connects directly to the aluminum box. The wire connected to the drain pin connects to the positive side of the capacitor bank.

The capacitor bank consists of ten capacitors, organized in two rows of five. The ten capacitors are wired in parallel by connecting each ten pins of corresponding polarizing with a piece of 18 AWG bus wire. The floating power supply BNC connector is connected to the four parallel 10Ω resistors. The other side of the resistors is then attached to the positive and negative sides of the capacitor bank via a two pin Molex connector. The positive side of the capacitor bank is connected to the drain pins of the MOSFETs, as previously mentioned. Another short section of 14 AWG stranded wire is connected to the negative side of the capacitor bank. This is the lead that connects to the negative valve electrode.

The leads that connect to the valve electrodes are as short as possible to minimize the resis-

tance and self-inductance of the circuit. Because of this, the box that houses the valve electronics must be mounted in close proximity to the valve itself. Two insulated ring terminals are soldered directly to the ends of the two leads. The connections to the valve are made between the ring terminals and the tops of the electrodes, which contain tapped holes to accommodate #6-32 screws (see Section 3.2.2.2).

A complete circuit diagram is depicted in Figure 2.4.

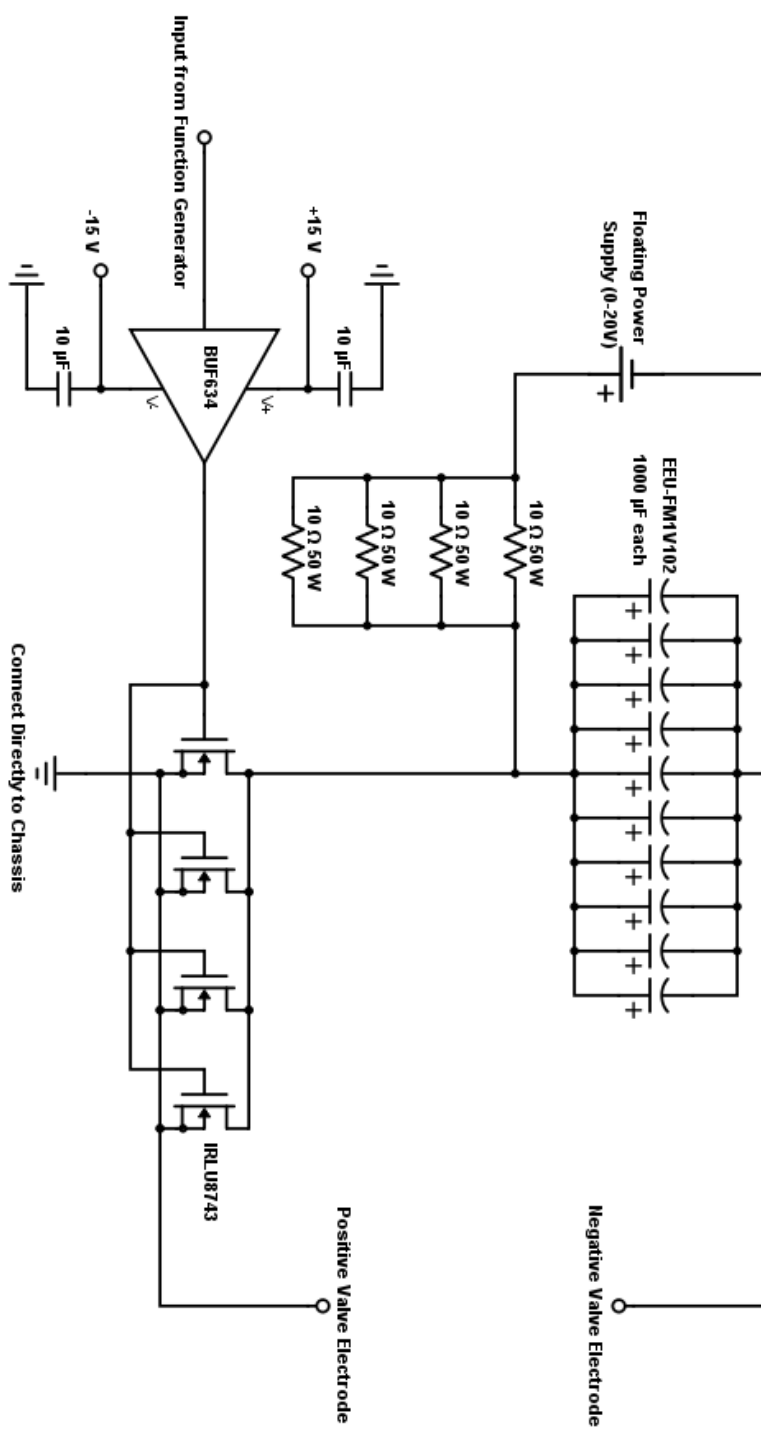


Figure 2.4: The full circuit diagram.

Chapter 3

Mechanical Design and Construction

At the most basic level, the mechanical operation of the valve involves a thin metal strip situated between two magnets. A small ball is attached to the bottom of the center of the strip. The ball seals against an O-ring that is centered on the nozzle. Custom electronics (see Chapter 2) designed to deliver a short-duration pulse of high current are connected to the valve via two electrodes. When high current is pulsed through the metal strip, it feels a Lorentz force upwards, opening the valve and allowing the gas to flow through the nozzle into vacuum. The design of the valve is based on the Nijmegen Pulsed Valve [19].

3.1 Design

The design of the valve consists of two major components: the **valve flange** (Figure 3.1) and the **valve body** (Figure 3.3). The valve flange acts as the front-end of the entire valve assembly—the front face is in contact with the vacuum, while the back face is in contact with the gas reservoir. The O-ring mounted on the back face is centered on a nozzle that goes directly through the center of the valve flange. The back face also contains a threaded insert for the valve body. The externally threaded valve body contains the electrodes, strip, and permanent magnets. The valve is sealed by screwing the valve body into the valve flange until the ball attached to the bottom of the strip makes a seal with the O-ring.

3.1.1 Valve Flange

The valve flange (see Figure 3.1) is custom machined from a blank double-side conflat vacuum flange to allow easy attachment to standard vacuum chambers. In fact, depending on the application, either face of the valve flange can; make a vacuum seal. When the valve is characterized in the testing chamber by measuring the time profile of the pulse of air molecules, the front face (the side opposite the threaded insert for the valve body) of the flange is sealed against the top flange of the chamber (see Section 4.2). When the valve is placed entirely in vacuum and used in conjunction with the deceleration experiment, the back face of the flange is sealed against the valve housing, creating the isolated gas reservoir.

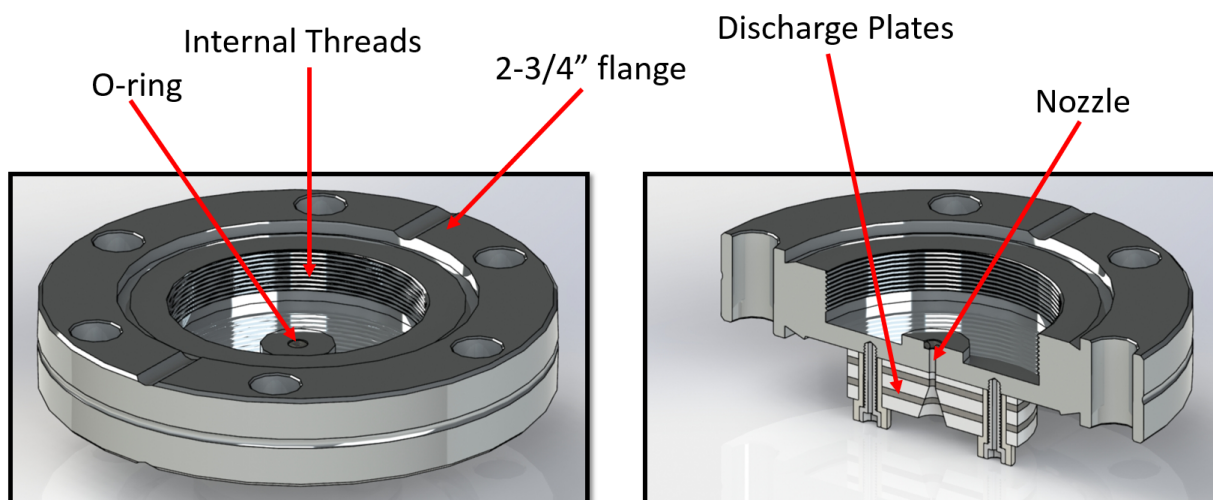


Figure 3.1: A SolidWorks rendering of the valve flange, with the different components labeled. The discharge plates and valve nozzle can be seen in the cross-sectional view.

The front face of the valve flange contains threaded holes for the attachment of discharge plates. The discharge plates consist of two conducting plates sandwiched between three insulators. The nozzle through the valve flange continues through the discharge plates. Other than ammonia, species of interest to use in cold molecule experiments are free radicals like the hydroxyl radical (OH). Free radicals are simple and relevant to things like combustion, atmospheric chemistry, and

interstellar chemistry. Discharge plates are used to create such free radicals. When producing a cold molecular beam of the OH radical, the gas reservoir is filled with water vapor (H_2O). When the valve opens, the water vapor expands through the nozzle. A large potential difference is applied to the plates, creating an electrical discharge that creates OH. The OH free radical that is produced then continues on to the further stages of the experiment.

An isolated gas reservoir is created when a metal housing is attached to the back face of the valve flange. Although this part has not been fabricated yet, its design consists simply of a sealed tube welded to a vacuum flange. The vacuum flange seals directly against the valve flange, enclosing the valve body within the tube. The back end of the sealed tube has through holes for the electrodes to make the electrical connections to the valve. The housing also contains an inlet to feed gas into the gas reservoir. The housing and how it attaches to the valve flange to create the gas reservoir is shown in Figure 3.2. With the housing attached, the valve assembly could be inserted completely into vacuum (see Figure 1.1).

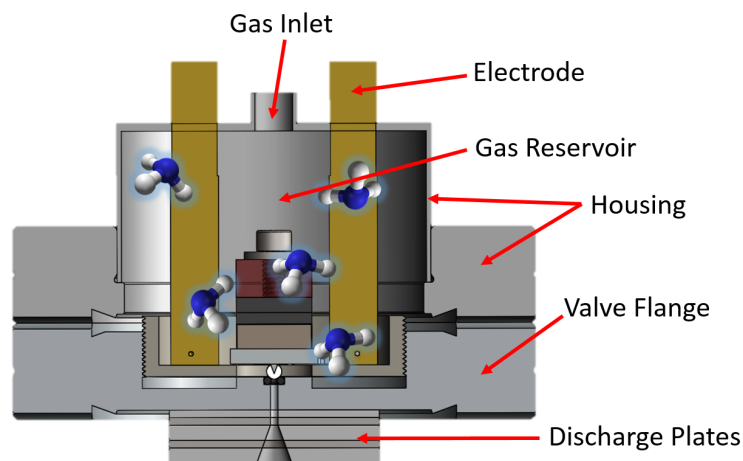


Figure 3.2: A cross-sectional view of the attachment of the valve housing. The vacuum flange seals directly against the valve flange, and the metal tube encloses the entire valve body, creating a sealed gas reservoir. Ammonia molecules are shown within the gas reservoir.

3.1.2 Valve Body

The valve body consists of several different components: the **base**, which is externally threaded to screw into the back face of the valve flanges; the **electrodes**, which make the electrical connections to the valve circuitry; the **strip clamps**, which connect the ends of the strip to the electrodes; the **strip**, which provides the opening and closing mechanism of the valve; and the **magnet assembly**, which aligns the two permanent magnets to straddle the center of the strip. Figure 3.3 depicts the geometry of the valve body.

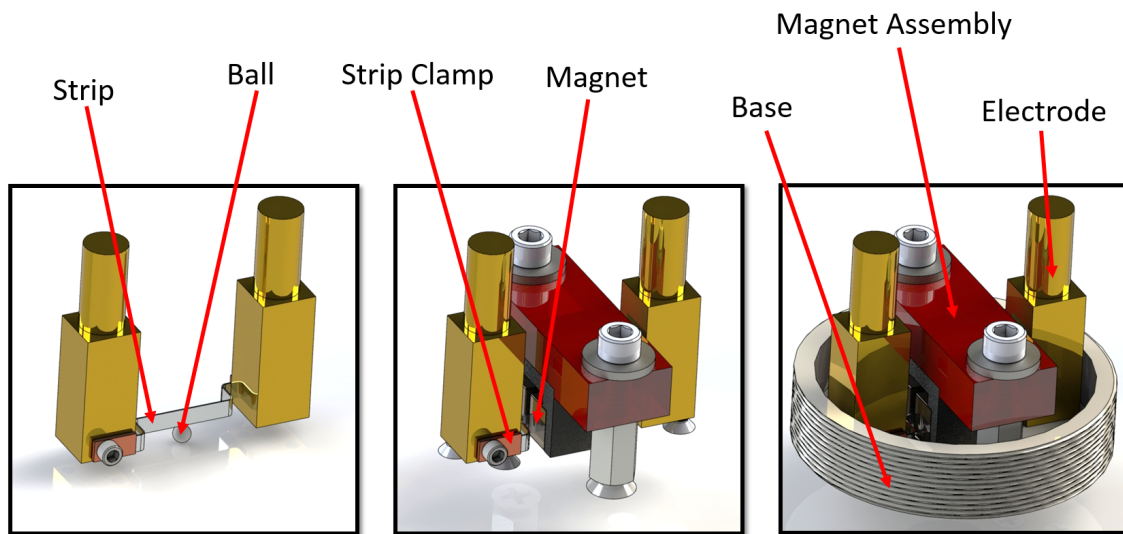


Figure 3.3: A SolidWorks rendering of the valve body, with the different components labeled. Some parts are hidden in the two views on the left to provide a view of interior components.

The various smaller components are attached to the base with screws. The electrodes are each connected with two screws so that they can be precisely aligned both translationally and rotationally. The bottom of the front face of each electrode contains a tapped hole that the strip clamps are screwed into. The ends of the strip are placed between the strip clamp and the electrodes, and the strip clamps are tightened down, fixing the ends of the strip to the electrodes.

The strip itself is bent into a zig-zag shape seen in Figure 3.3. Since the strip is fixed at either end, it springs back downwards by its own spring force after the current stops. The shape of

the strip causes most of the elastic deformation to occur in the bends perpendicular to the center section of the strip, allowing the center section to move upwards naturally. (It is important that the center of the strip, where the ball is attached, moves directly upwards away from the O-ring and springs back along the same path so that the valve is resealed as quickly as possible.) The shape of the strip also allows small motions in both directions perpendicular to its opening motion. This way, if the ball is not exactly centered on the O-ring (this imprecision is usually caused by the manufacturing process of the strip and the ball—see Section 3.2.2.4), this small amount of positional freedom allows it to self-center.

Also attached to the base is the magnet assembly. The magnet assembly consists of the two permanent neodymium magnets, the **magnet yoke**, and the **magnet bracket**. The two permanent magnets are glued directly into the iron magnet yoke, which serves two purposes. First, it sets the gap distance between the magnets at two millimeters, which is small enough to keep a strong magnetic field within the gap, but large enough to accommodate the center section of the strip. Second, it contains the magnetic field lines emanating from the faces of the magnets opposite the gap, strengthening the magnetic field within the gap [8]. The magnet yoke is glued onto the magnet bracket, which aligns the entire magnet assembly with the holes on the base that are used to attach it with two hex standoffs.

The dimensions of the permanent magnets are 4x5x10 mm, with the 10 mm dimension along the length of the strip and the 5 mm dimension along the direction of the strip movement. The Lorentz force experienced by a wire carrying current in a magnetic field is

$$\vec{F} = \vec{I}l \times \vec{B}, \quad (3.1)$$

where \vec{I} is the current (in this case, 1600 A in the direction of the strip), l is the interaction length (roughly 10 mm), and \vec{B} is the magnetic field. The magnetic field and current vectors are perpendicular, and the cross product of the two unit vectors associated with these directions is a unit vector in the direction of the strip movement. Although the magnetic field has not been measured

directly, it can be estimated using a magnetic gap calculator [8]. To simplify the calculation, the block magnets are idealized as two cylindrical magnets with a diameter of 7 mm (the thickness and gap distance remain the same at 4 mm and 2 mm, respectively). The model gives a value of magnetic field magnitude at the center of the gaps as $B \approx 1$ T (without the magnet yoke, the model yields $B \approx 0.75$ T). Using this value of the magnetic field, and the maximum current produced of 1600 A, the force experienced by the strip is $F = 16$ N. This exceeds the 7 N force experienced by the Nijmegen Pulsed Valve [19]. Of course, the force can be reduced if necessary by dialing down the voltage on the floating power supply, producing a pulse with a lower peak current.

3.2 Construction

One of the advantages of this valve design is that it can be built in-house for relatively low cost. The machining, though not trivial, could be performed by any ambitious experimentalist familiar with common metalworking tools (e.g., mill, lathe, bandsaw). This section contains step-by-step instructions and technical drawings to aid in the fabrication of each component.

3.2.1 Valve Flange

The valve flange is machined from a 2-3/4" Conflat flange blank. The flange chosen is double-faced, meaning it has a knife edge to make a vacuum-tight seal on both faces. On the front face, the valve flange has two #2-56 bottom tapped holes for attaching the discharge plates. The back face has a threaded insert (1.375"-40) for the valve body and a small bore in which the O-ring is seated. A 1 mm nozzle connects the two faces. Here are the parts needed:

- 2-3/4" Conflat Flange Double-Faced Blank (Kurt Lesker P/N DFF275X000)
- Size 001 Viton O-ring (McMaster P/N 9464K101)

The part is machined using the following steps (see Figure 3.4):

- (1) Set the part up on the lathe using a vacuum flange collet
- (2) Create the large 1.36" bore

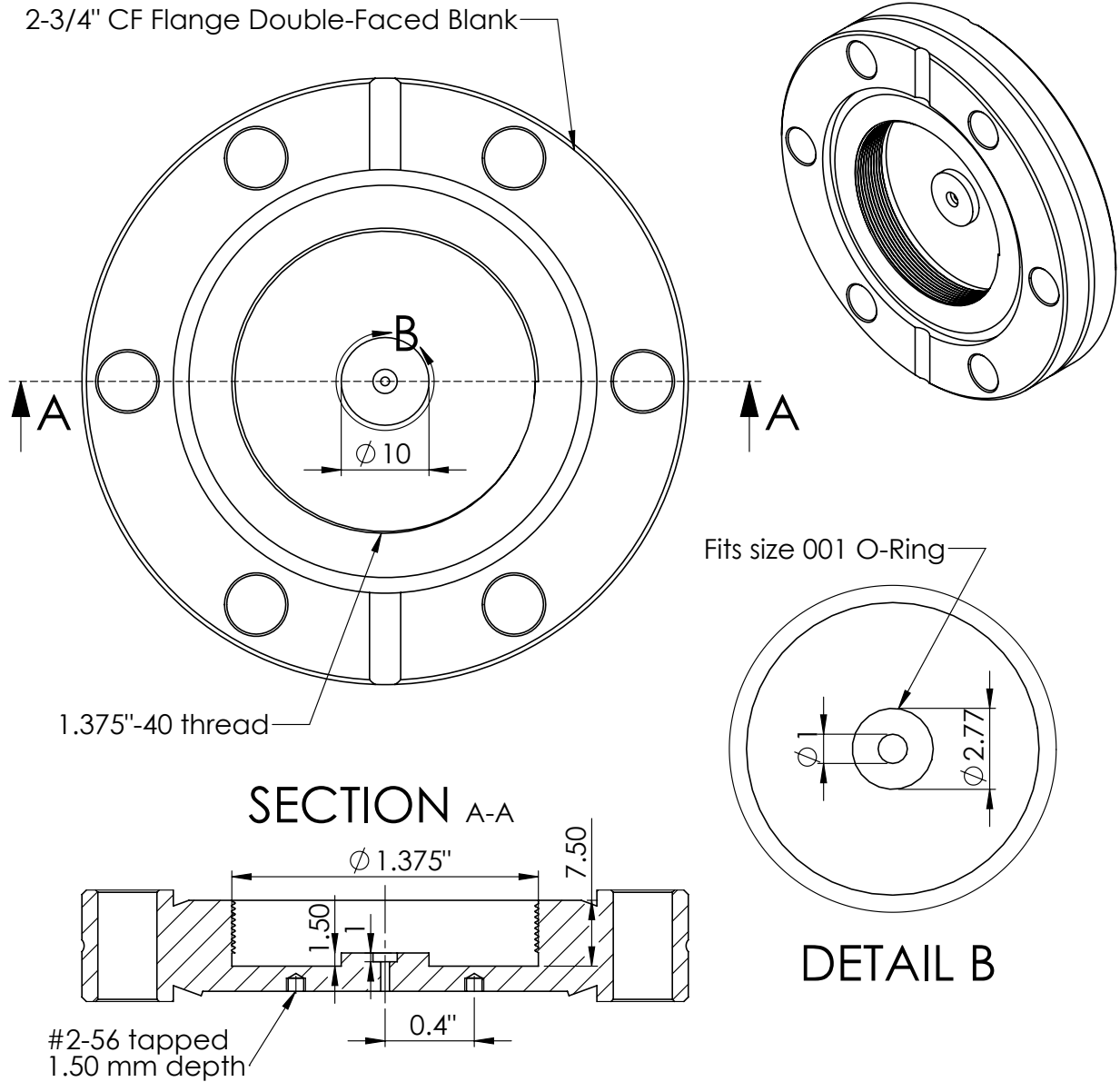


Figure 3.4: The SolidWorks drawing of the valve flange. All dimensions are in mm, unless otherwise noted.

- (3) Make the small bore to fit the O-ring
- (4) Drill the 1 mm nozzle through the flange
- (5) Create a small undercut near the bottom of the large bore
- (6) Set the feed rate on the lathe to cut 40 threads per inch
- (7) Using a threading tool, cut the threads down to the undercut
- (8) Set up the part on the mill and center it using a dial indicator
- (9) Drill and tap the #2-56 holes (be careful not to punch through to the other side, the tolerance is tight)

After the part is cleaned, the O-ring is press fit into the small bore. If the O-ring bore is precisely machined, the O-ring will fit tightly without deforming, and seal with the Torr Seal ball described in Section 3.2.2.4.

3.2.2 Valve Body

The valve body consists of the base, electrodes, strip clamps, strip, and magnet assembly.

3.2.2.1 Base

The base precisely aligns the electrodes and magnets, and ensures that the Torr Seal ball is centered over the O-ring seated in the valve flange. Although doing so somewhat complicates the machining process, the smaller components are inset inside the base in order to minimize the length of the nozzle. External 1.375"-40 threads are cut into the outer cylindrical face, allowing the base to screw into the valve flange and finely adjust the closing tension of the valve. The base is machined from PEEK, a vacuum compatible and high-temperature resistant plastic. Of course, the base must be an electrical insulator so that the electrodes are isolated.

Here are the parts needed:

- 1-1/2" diameter PEEK rod (McMaster P/N 7269K22)
- Nylon 5C emergency collet, custom-machined to fit 1.375" diameter piece
- Finished valve flange to check thread fit

The finely cut threads on the exterior of the base are fragile. For this reason, holding it in the lathe with a standard steel collet is not recommended once the threads have been cut. Instead, a nylon collet is used. If a nylon collet of the proper size is not on hand, this piece can be fabricated by first inserting a taper pin into the center of the collet to spread the jaws and then using a boring bar on the lathe to bore 1.375" diameter to at least 5 mm depth.

The part is machined using the following steps (see Figure 3.5):

- (1) Using the bandsaw, cut off approximately 15 mm of the 1-1/2" PEEK rod
- (2) Using a lathe chuck to hold the piece, face off both ends of the piece and turn the last 5 mm of one end to a diameter of 1 inch
- (3) Use a 1" steel 5C collet to hold the 1" end of the piece and turn the outer diameter of the other end of the piece to 1.372" (slightly under the nominal diameter of the threads)
- (4) Bore out the center of the piece to a diameter of 30.5 mm and a depth of 6.5 mm
- (5) Create the 10 mm hole through the center of the entire piece (drill a rough 9 mm hole before drilling the 10 mm hole)
- (6) Set the feed speed of the lathe to cut 40 threads per inch
- (7) Chamfer both ends of the protruding piece
- (8) Cut the threads with a threading tool, making sure to cut only five thousandths of an inch with each pass
- (9) Once the threads start to form, check the fit between the base and the valve flange after each pass
- (10) Once the valve flange threads tightly but smoothly onto the base, the threads are complete (this occurs after cutting the threads to a depth of approximately 0.030")
- (11) Remove the piece from the lathe, keeping it in the collet, and use the collet block to set it up on the mill
- (12) Use a dial indicator on the cylindrical inner wall of the piece to zero the center of the part (the accuracy in this step is crucial)
- (13) Drill the holes for attaching the electrodes (#48 drill) and the magnet assembly (#32 drill)
- (14) Remove the piece from the mill and set it up on the lathe with the custom nylon collet so that the 1" piece is protruding out (clamping the piece too tightly runs the risk of damaging the threads)
- (15) Turn down the 1" diameter piece and the length of the threaded section until the piece is 8 mm long

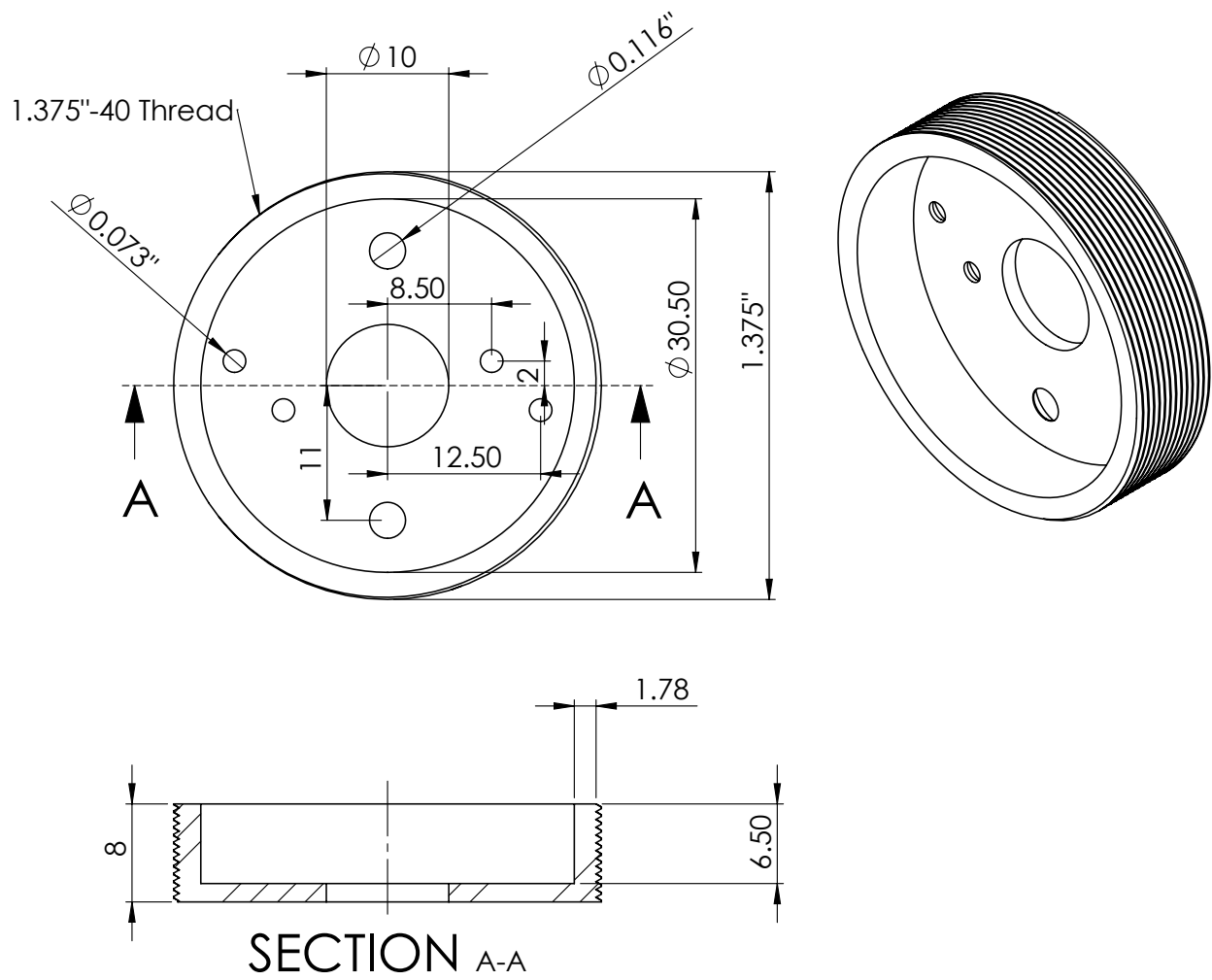


Figure 3.5: The drawing of the base. All dimensions are in mm, unless otherwise noted.

- (16) Re-chamfer the end of the piece that has been cut down
- (17) Remove the piece from the lathe, keeping it in the nylon collet, and set it up on the mill with the collet block
- (18) Using an 82° countersink, countersink the through-holes for the screws that attach the electrodes and magnet assembly
- (19) Take the piece off the mill and finish it by deburring the holes and sanding the inside bottom face with fine grit sandpaper

After the piece is finished and cleaned, it should be able to thread smoothly into the valve flange. Because of the fragility of the plastic threads, there is a possibility of the pieces threading together incorrectly, resulting in two of the threads being pushed together. This problem can be fixed by lightly filing along the path of the threads with a small triangular file.

3.2.2.2 Electrodes

The electrodes serve to connect the strip to the leads from the electronics that supply the high current pulse and to align the strip so that the ball attached to its center seals well against the O-ring. The bottom of each electrode has two #1-72 tapped holes in opposite corners to attach it to the base (two screws are necessary to remove the rotational freedom of the electrodes). The bottom of the front face of each electrode has a #0-80 tapped hole used to clamp the strip against it. The #6-32 tapped holes on top of the electrodes are used to connect the ring terminals from the electronic leads. Brass is chosen as the electrode material because of its high-conductivity and ease of machinability.

Here are the materials needed:

- 1/4" x 1/4" square brass stock (McMaster P/N 8951K13)

Each electrode is machined using the following steps (see Figure 3.6):

- (1) Cut a little more than 25 mm from the brass stock with the bandsaw
- (2) Set up the piece on the lathe with a 1/4" square collet
- (3) Face off both ends and turn the length down to 25 mm

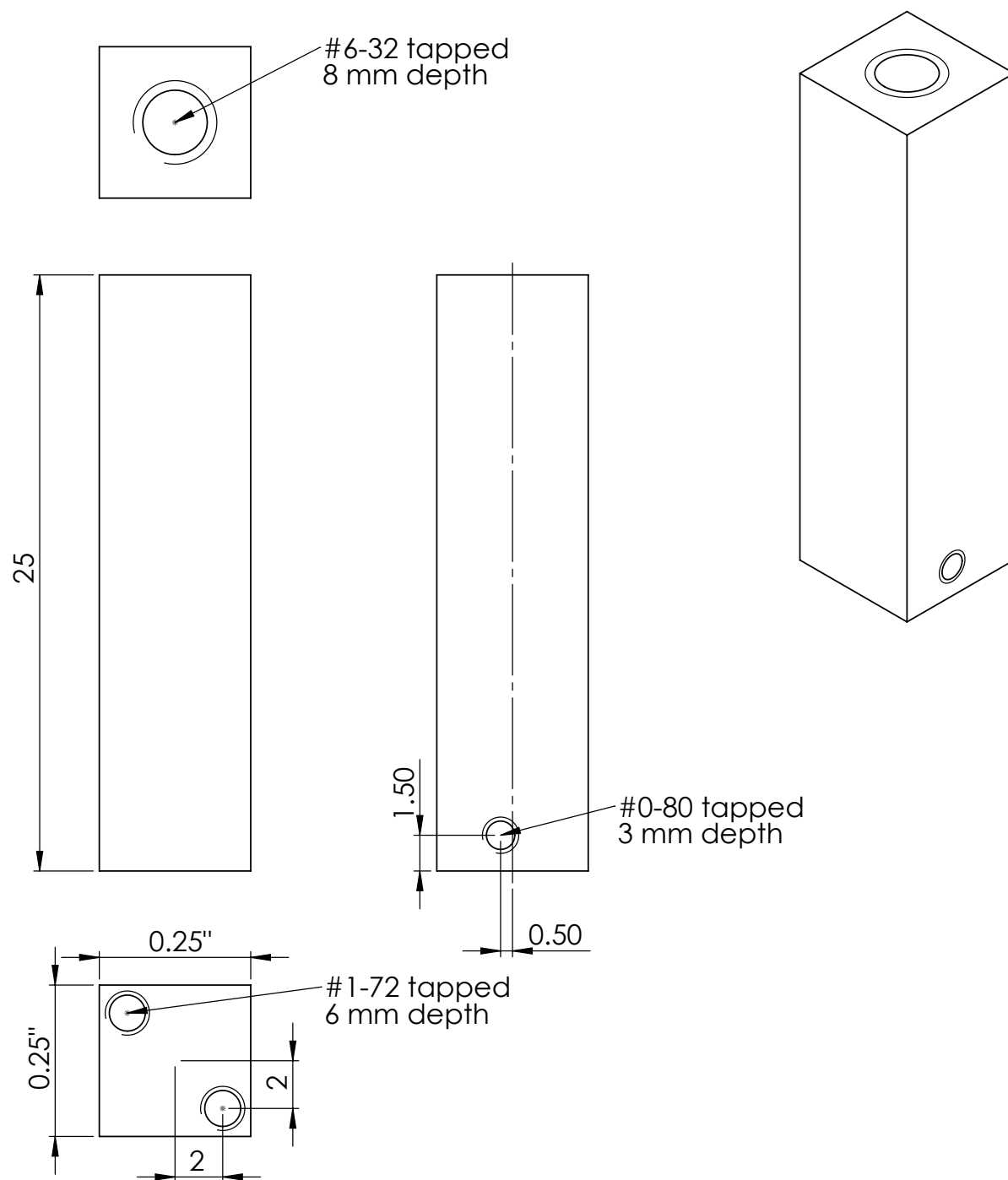


Figure 3.6: The drawing of an electrode. All dimensions are in mm, unless otherwise noted.

- (4) Drill and tap the #6-32 hole in the center of one end of the piece
- (5) Set up the piece on the mill so that the face opposite the newly tapped hole is facing upward
- (6) Drill and tap the two #1-72 holes
- (7) Realign the piece in the vise and create the #0-80 tapped hole

3.2.2.3 Strip Clamps

A strip clamp is nothing more than thin, rectangular copper piece with a #0-80 through hole near one end. As the name might suggest, the strip clamps are used to clamp either end of the strip tightly against the electrodes. The strip clamps are machined from 1 mm copper sheet (McMaster P/N 8963K162).

The strip clamps are machined using the following steps (see Figure 3.7):

- (1) Use calipers to scribe the copper sheet, marking a line of rectangles 4 mm tall and 7 mm wide
- (2) Use calipers to mark dots in the center of the line 2 mm from the left side of each rectangle
- (3) After clamping the piece down, use the drill press to drill #0-80 through holes (#52 drill) at each of the dots marked in the previous step
- (4) Shear off the line of rectangles from the rest of the copper sheet and then shear each rectangle from the line (the result is several oversized strip clamps)
- (5) Working one at a time, use pliers to hold the small piece and grind down each side until reaching the dimensions prescribed by the drawing

Although copper has the advantage of being highly conductive, it is also a relatively soft metal. The thin strip clamps thus have a tendency to bend slightly. When installing a new strip, the each strip clamp should be flipped so that the ends are bent towards the electrode.

3.2.2.4 Strip

The performance of the strip is highly coupled to the specific material chosen. To create the best valve possible, the material chosen must be conductive, lightweight, springy, and durable. The best material found is Aluminum 4043 alloy (94% aluminum, 5% silicon, 1% other metals).

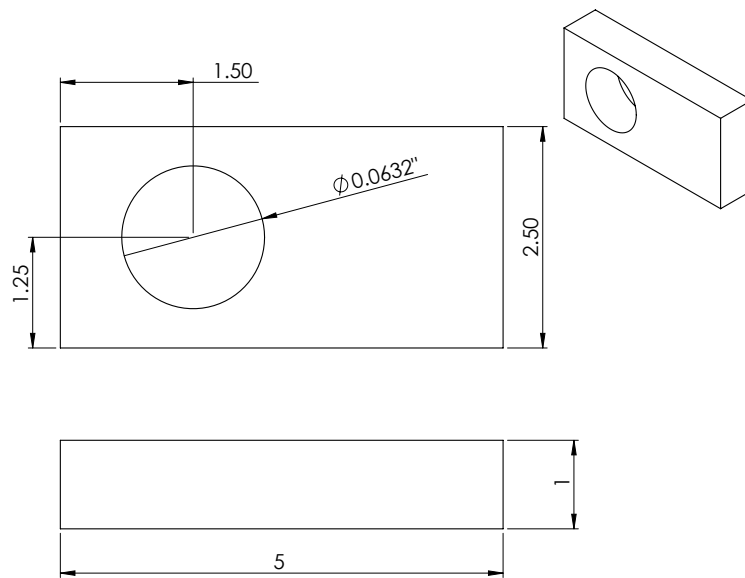


Figure 3.7: The drawing of a strip clamp. All dimensions are in mm, unless otherwise noted.

Aluminum 4043 is only commercially available in welding rods. However, it is a relatively easy task to use a rolling mill to roll the welding rods into sheets 0.006" thick. Then, using shears, these sheets are then cut into small strips 4 mm tall and 25 mm wide. Next, the strips are carefully cut with scissors so that a 2 mm square protrudes from the bottom (see Figure 3.8).

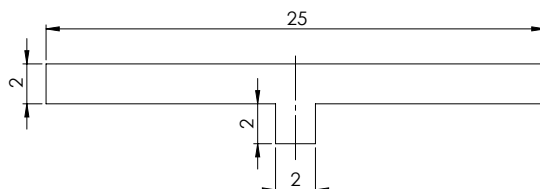


Figure 3.8: The aluminum strips are cut out with a 2 mm section protruding from the bottom. This section is then crimped together to form a triangular shape. All dimensions in mm.

The sides of the square tab protruding from the bottom of the strip are then crimped together to form a roughly triangular shape. This step, as opposed to simply cutting off the corner of the square to form a triangular protrusion, serves the purpose of increasing the texture and surface area where the ball is connected.

The ball is formed directly onto the triangular tab with Torr Seal, strong epoxy typically used as a vacuum sealant. The process is as follows:

- (1) In the fume hood, mix together the two parts of the Torr Seal in the standard ratio indicated
- (2) Plug in a soldering iron and turn it on
- (3) Use the alligator clips on a soldering stand to hold the strip up with the triangular tab facing directly downwards
- (4) With a small wooden stick or needle, pick up a small portion of mixed Torr Seal and apply it evenly around the bottom half of the triangular tab (the exact shape of the Torr Seal glob is unimportant)
- (5) Hold the hot soldering iron directly beneath the glob of Torr Seal for at least ten seconds (it is necessary to directly touch neither the Torr Seal nor the metal strip directly with the soldering iron)
- (6) After the Torr Seal heats up, its surface tension will cause it to smooth out (the bottom of the Torr Seal ball should be hemispherical and about 2 mm in diameter—if the ball doesn't form well, simply use a delicate task wipe to remove the glue and try again)

- (7) Gently place the strip into a drying rack with the Torr Seal ball facing down and allow to dry for a full day

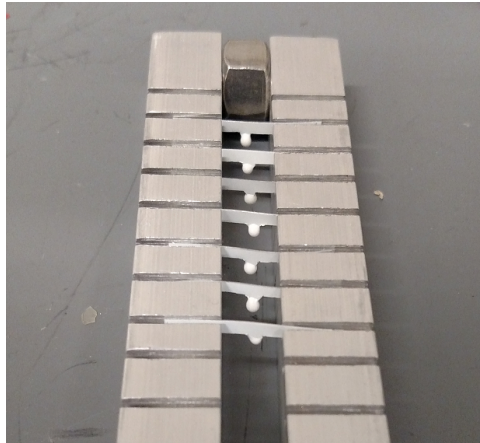


Figure 3.9: The strips are left for 24 hours to allow the Torr Seal to dry. The drying rack is machined by clamping together two aluminum bars and cutting several slots with a horizontal bandsaw.

Once the strips have been allowed to dry, they are ready to be bent into shape and installed in the valve assembly. Bending is a reproducible process thanks to the advent of the strip bending jig, a flat piece of aluminum with removable pins precisely located to produce a bent strip of the proper dimensions. The center of the jig contains a small hole that the ball fits into, ensuring that the ball is always in the center of the bent strip. The strip bending jig is machined from a small rectangular piece of scrap aluminum using the following steps:

- (1) On the mill, face off the smaller four faces of the aluminum block with a large end mill
- (2) Face off the large two faces of the piece with a fly cutter
- (3) Pick an arbitrary (0, 0) point near the center of the block
- (4) Drill holes slightly under with a #62 drill (slightly under 1 mm in size) in the following four locations, in mm, relative to the centerpoint: (-6.65, -2.68), (-5.50, -0.58), (5.50, 0.58), and (6.65, 2.68)
- (5) Use a 1 mm metric reamer to ream out each of the four holes
- (6) Drill a 3 mm hole at least 4 mm deep in the center of the block
- (7) Fit 1 mm metric dowel pins into each of the four smaller holes, making sure that they extend at least 3 mm from the surface of the aluminum

To bend the strip in the jig, the center to pins are first inserted. The strip is placed on the jig by centering the ball in the larger hole. Each side of the strip is then bent 90 degrees around the corresponding pin. The outer two pins are then inserted into the jig and used to bend each end of the strip 90 degrees back; the strip is now in its final form. The use of dowel pins in the design of the bending jig is crucial because they form smooth bends in the strip with a bend radius of 0.5 mm. Sharp bends are weaker because the material has been stressed, drastically reducing the lifetime of each strip. Figure 3.10 shows a strip in the bending jig, and Figure 3.11 shows a collection of finished strips.



Figure 3.10: A view of the strip in the bending jig. The Torr Seal ball lines up with the hole in the center.

3.2.2.5 Alignment Plate

Because of the tight geometry of the valve body, it is impossible to fit in a screwdriver to tighten the small screws that clamp the strip against the electrodes when they are mounted in the base. The alignment plate provides a way to attach the strip to the electrodes in the proper position before these pieces are installed within the base. The alignment plate has through holes for connecting the electrodes in identical locations to those on the base, as well as a 3 mm hole to center the ball.

The part is machined using the following steps:

- (1) On the mill, face off the smaller four faces of an aluminum block with a large end mill

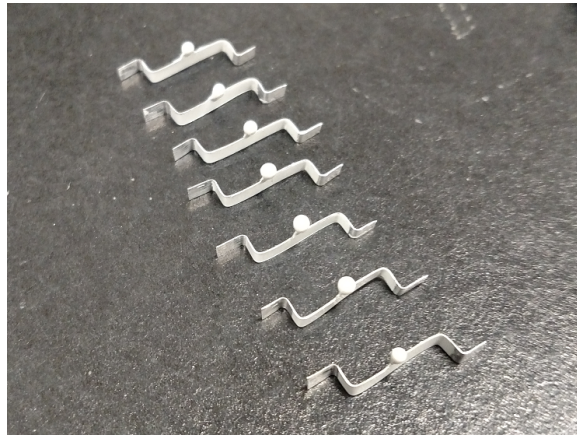


Figure 3.11: A collection of finished strips.

- (2) Face off the large two faces of the piece with a fly cutter
- (3) Drill the #1-72 through holes for the electrode screws (#48 drill) and the 3 mm hole in the center
- (4) Use an endmill to mill the outer sections of the aluminum piece and create the 0.5 mm boss in the center (this boss sets the distance between the bottom of the strip and the base so that the two do not touch)

3.2.2.6 Magnet Assembly

The magnet assembly consists of four distinct parts—the magnets themselves, the magnet yoke, the magnet bracket, and hex standoffs that raise the aforementioned parts above the base.

Here are the materials used:

- Grade N42 NdFeB magnets, 10x5x4 mm
- 1/2" thick easy-to-machine cast iron bar (e.g., McMaster P/N 8928K48)
- 1/4" thick acrylic sheet (e.g., McMaster P/N 8505K91)
- #4-40 threaded hex standoffs, 5/16" length (McMaster P/N 90308A607)

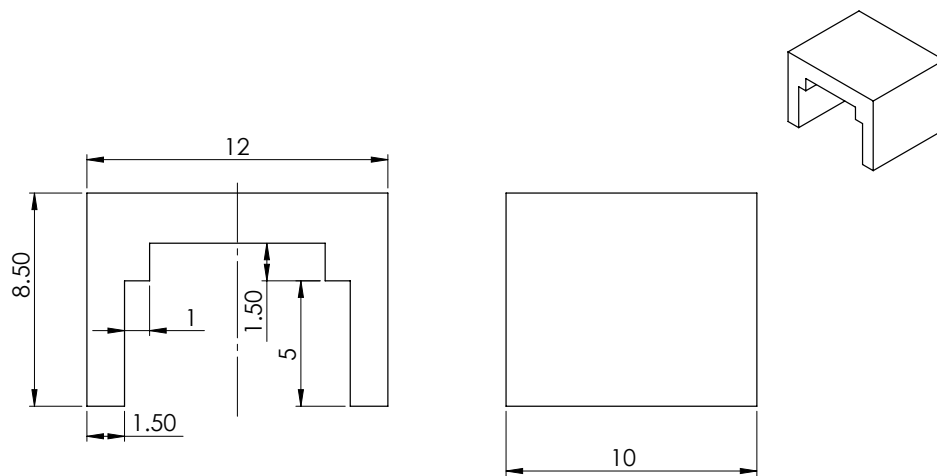


Figure 3.12: The SolidWorks drawing of the magnet yoke. All dimensions are in mm, unless otherwise noted.

The magnets are glued directly into the magnet yoke, which sets the gap distance at 2 mm. The magnet yoke also serves the purpose of increasing the magnetic field strength within the gap.

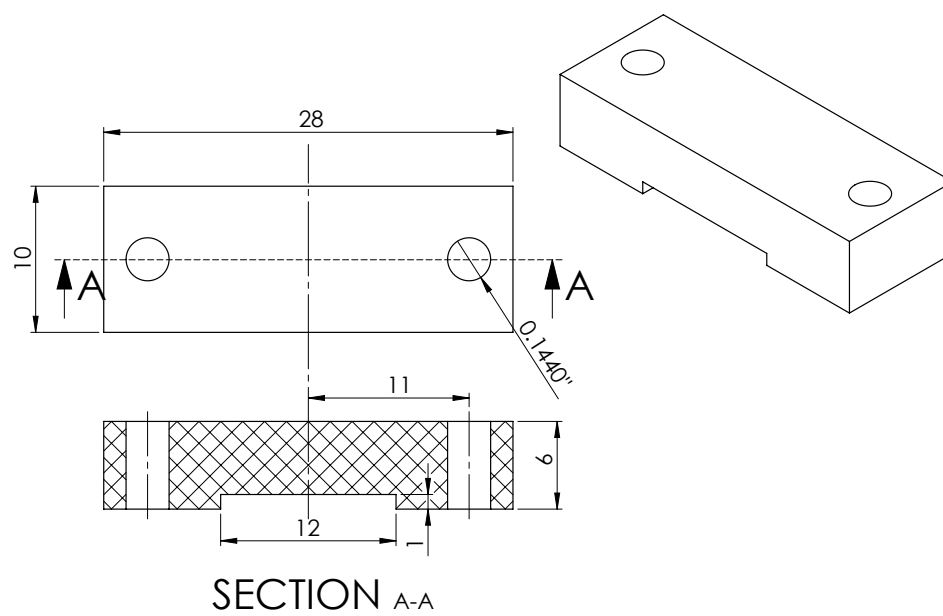


Figure 3.13: The SolidWorks drawing of the magnet bracket. All dimensions are in mm, unless otherwise noted.

The magnet yoke is machined using the following steps (see Figure 3.12):

- (1) Use the bandsaw to cut off a piece of cast iron approximately 10x12 mm large
- (2) Set up the piece on the mill and use an endmill to square off the sides and reduce the dimensions to 8.5x10x12 mm
- (3) Realign the piece in the vise so that one of the 10x12 mm faces is pointed upwards, and use the endmill to cut out the shape indicated in the drawing

To attach the magnets to the magnet yoke, and 1 mm thick metal spacer is placed between the magnets. Then, the magnets are glued into the magnets yoke using Armstrong A-12 epoxy resin (Ellsworth P/N A-12 C-KIT) and allowed to cure for 24 hours.

The magnet bracket is a simple acrylic piece that attaches to the magnet yoke and the hex standoffs connected to the base. The piece is machined as follows (see Figure 3.13):

- (1) Use the bandsaw to cut off a piece of acrylic approximately 12x30 mm
- (2) Set up the piece on the mill and use an endmill to square off the sides and reduce the dimensions to 10x28 mm (leave the 1/4" thickness uncut)
- (3) Drill the two #4-40 through holes (#32 drill)
- (4) Use an endmill to cut out the inset for the magnet yoke

The magnet bracket is glued directly to the magnet yoke, again using Armstrong A-12 epoxy resin, and allowed to cure. Once the epoxy has dried, the magnet assembly is ready to be attached to the base via the hex standoffs.

3.2.3 Full Assembly

The parts are cleaned ultrasonically before they are assembled. The valve flange is cleaned directly in a solution ofalconox laboratory detergent. The smaller components of the valve body, on the other hand, are placed in a separate beaker full of deionized water before they are dipped in the ultrasonic cleaner.

Once the parts have been cleaned, the valve body can be assembled. The fasteners used in the assembly of the valve body are shown in Table 3.1. To avoid contamination, the parts are

Table 3.1: Fasteners used in valve assembly

Fastener	Quantity	McMaster P/N
#0-80 Pan Head Phillips 1/8"	2	91772A052
#1-72 Flat Head Phillips 3/16"	4	91771A165
#1-72 Pan Head Phillips 3/8"	4	91772A068
#4-40 Flat Head Phillips 3/16"	2	91500A120
#4-40 Socket Head 5/16"	2	92196A107
#6-32 Socket Head 1/4"	2	92196A144

assembled on a clean surface (UHV foil placed on a lab bench works nicely) while wearing gloves.

The valve body is assembled in the following manner:

- (1) Use the #1-72 pan head screws to attach the electrodes to the alignment plate, ensuring that the #0-80 tapped holes are facing the right direction to align with the ends of the strip
- (2) Attach the strip clamps to the tapped holes near the bottoms of the electrodes with the #0-80 pan head screws
- (3) Slip the ends of the strip between the each electrode the the strip clamp and tighten down the strip clamps after centering the Torr Seal ball in the hole in the center of the alignment plate
- (4) Unscrew the #1-72 pan head screws attaching the electrodes to the alignment plates
- (5) With the #1-72 flat head screws, attach the electrodes to the base
- (6) Push the ball into place if it is slightly off-center
- (7) Attach the hex standoffs to the base with the #4-40 flat head screws
- (8) Attach the magnet assembly to the hex standoffs with washers and the #4-40 socket head screws

After the valve body is assembled, it is simply screwed into the valve flange. The #6-32 socket head screws are used to connect the ring terminals from the electronics to the tapped holes in the tops of the electrodes. The valve body assembly is depicted in Figure 3.14, and the full valve assembly is depicted in Figure 3.15.

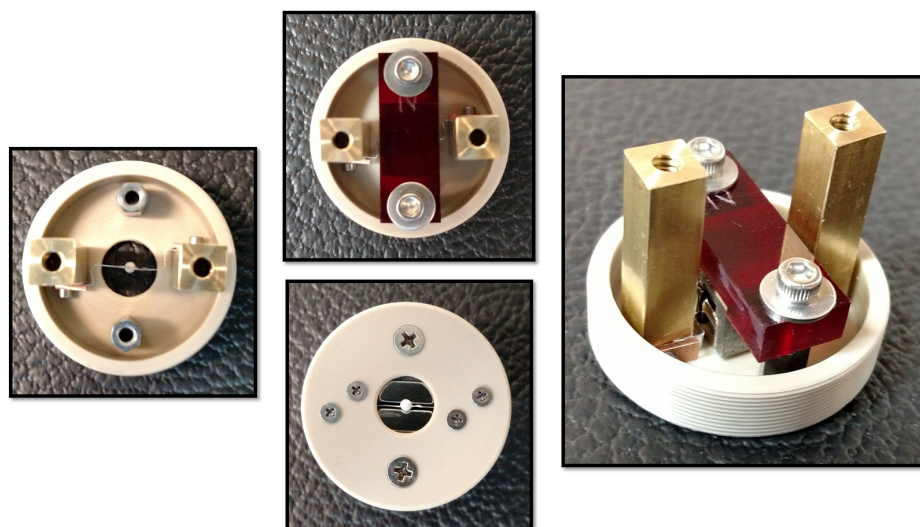


Figure 3.14: Several views of the assembled valve body. In the left most view, the magnet assembly is removed.

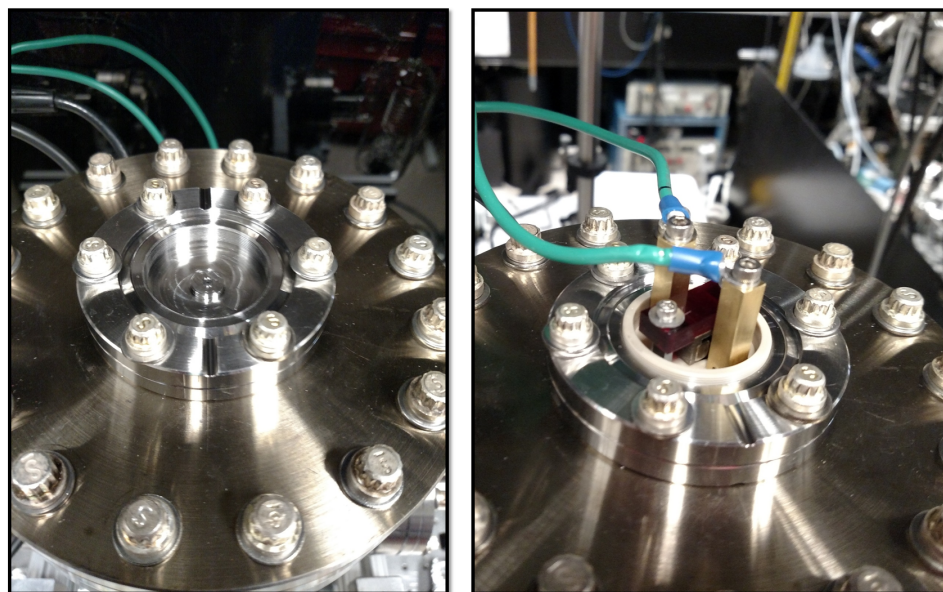


Figure 3.15: Views of the valve flange attached to the testing chamber, with and without the valve body attached.

Chapter 4

Methods of Valve Characterization

This describes two different methods used to measure the performance of the new valve. The first is the mechanical motion test, in which the displacement and speed of the valve strip are directly measured. The second is the gas pulse test, in which the characteristics of a pulse of air molecules created by the valve are measured.

4.1 Mechanical Motion

In the mechanical motion test, a helium-neon (HeNe) laser is used to characterize the speed and displacement of the metal strip. The motion of the strip itself does not directly map onto the properties of the gas pulse produced by the valve. However, qualitatively, a strip that moves faster and farther will create a gas pulse that is denser and shorter duration. The mechanical motion test is used to determine the relative behavior of the valve for several different parameters like driving pulse length and strip material.

One should note that the geometry of the the valve assembly described in Chapter 3 prohibits the use of this kind of test because there is no straight line path perpendicular to the strip along which to direct a laser beam. This test was performed on an earlier prototype of the valve (see Figure 4.1) without this geometrical restriction. There are several design differences between this older prototype and the current version of the valve (e.g., slightly different strip dimensions and different interaction lengths between the strips and the magnets). However, again, this does not invalidate the mechanical motion test as a relative measure of the performance of the valve across a

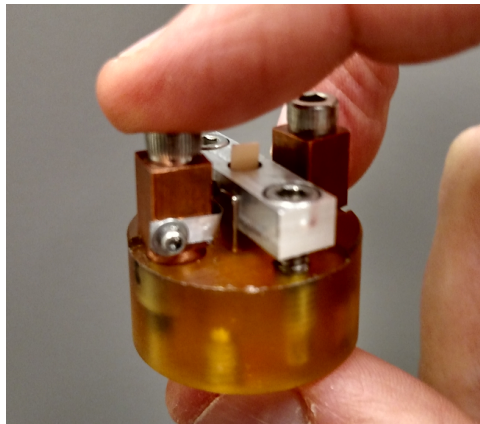


Figure 4.1: Shown here is an early prototype of the valve, used in the mechanical motion test. A small plastic tab is glued to the center of the strip and extends vertically past the magnet assembly, allowing the motion of the center of the strip to be determined by shining a laser beam perpendicularly to the tab and measuring the change in laser power incident on a photodiode during the strip's motion.

vast parameter space. Note that the earlier prototype of the valve also lacks a sealing mechanism. Since there is nothing to damp the motion of the strip, the strip continues to oscillate in the displacement versus time curves retrieved using this method.

The mechanical motion test is based on the razor blade technique of characterizing laser beams with Gaussian intensity profiles. In the razor blade technique, a translation stage is used to move a razor blade into the path of a laser beam in small increments. A photodiode is used to measure the total laser power as a function of razor blade position, characterizing the intensity profile of the beam. A plastic tab affixed to the top of the valve strip blocks the laser light in a similar way to the razor blade. The measurements of the laser power on the photodiode during the strip's motion can be used to quantify the speed and displacement of the valve strip.

The intensity of a Gaussian laser beam propagating in the z direction is [18]

$$I(x, y, z) = \frac{2P_0}{\pi\omega(z)^2} \exp\left(\frac{-2(x^2 + y^2)}{\omega(z)^2}\right), \quad (4.1)$$

where P_0 is the total power of the beam,

$$P_0 = \int_{-\infty}^{\infty} \int_{-\infty}^{\infty} I(x, y) dx dy, \quad (4.2)$$

and $w(z)$ is the beam radius. The beam radius is defined as the distance from the center of the beam where the intensity has dropped by a factor of e^2 . As a razor blade is moved up along the y -axis, it begins to block the laser beam. The laser power incident of the photodiode, $P(y)$, is then given by the difference between the total laser power, P_0 , and the laser power blocked by the razor blade, $P_b(y)$:

$$P(y) = P_0 - P_b(y) = \int_{-\infty}^{\infty} \int_{-\infty}^{\infty} I(x, y', z) dx dy' - \int_{-\infty}^y \int_{-\infty}^{\infty} I(x, y', z) dx dy'. \quad (4.3)$$

After some algebra, this leads to the result

$$P(y) = \frac{P_0}{2} \left(1 - \operatorname{erf}\left(\frac{y\sqrt{2}}{\omega(z)}\right) \right), \quad (4.4)$$

where $\text{erf}()$ is the error function. Of course, the y -value that the razor blade starts at is arbitrary. This is incorporated into the equation by introducing the offset y_0 :

$$P(y) = \frac{P_0}{2} \left(1 - \text{erf} \left(\frac{\sqrt{2}(y - y_0)}{\omega(z)} \right) \right). \quad (4.5)$$

The laser beam is profiled by measuring the power incident on the photodiode as a function of razor blade position and fitting these data points to the equation above. In practice, the power of the laser is not directly measured. The photodiode converts light into current (the current is directly proportional to the power of the light source). A transimpedance amplifier is then used to convert the current into voltage, which is simply read from an oscilloscope.

The experimental set-up consists of a HeNe laser, a translation stage, and the photodiode. Both the razor blade and the valve can be mounted on the translation stage so that the laser beam intersects them at the same location. This ensures that the intensity profile is the same in both cases, even if the laser beam is not exactly collimated.

The HeNe laser outputs a collimated beam of red laser light with a beam radius of $\omega \approx 0.8$ mm. This beam radius proves to be an appropriate size to measure the displacement of the strip (on the order of $200 \mu\text{m}$). If the valve is aligned so that the top of the strip is near the center of the laser beam, the strip movements remain within the roughly linear regime of the error function curve, and the changes in the voltage reading on the oscilloscope are approximately proportional to changes in strip position. In other words, the pulse shape seen on the oscilloscope is a close approximation to the real shape of the displacement versus time curve. To find the displacement versus time curve from the voltage versus time curve retrieved from the oscilloscope, the slope (change in voltage per change in position) of the error function fit curve (Figure 4.2) is used to convert the voltage to an arbitrary position. Then, the displacement versus time curve is determined by shifting this position versus time data so that the resting position of the strip is defined as zero displacement.

First, the intensity profile is measured by moving the razor blade mounted on the translation stage vertically into the path of the laser beam and recording the voltage seen on the oscilloscope

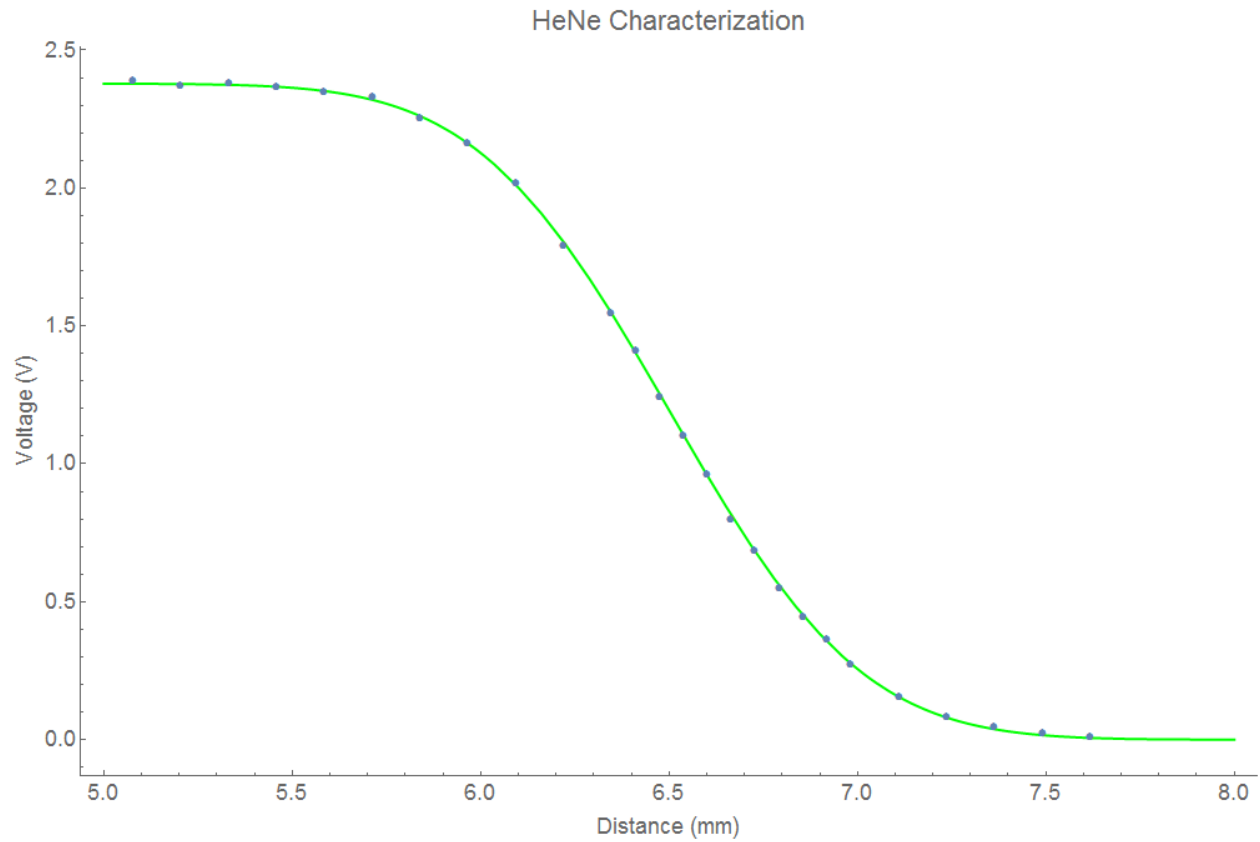


Figure 4.2: By measuring the minimum and maximum voltages seen on the oscilloscope during the motion of the valve strip, we can determine the displacement. The voltage seen on the oscilloscope at the top and bottom of the strip's movement are matched to voltages on this intensity profile plot, quantifying the displacement. If the motion of the valve strip remains in the linear regime at the center of this curve, the voltage versus time plot returned by the oscilloscope can be transformed into a displacement versus time plot.

(which is, again, proportional to the power incident on the photodiode). Then, using *Mathematica*, the data points are plotted and fit to the error function curve given by Equation 4.5. From the error function fit, the variables P_0 , y_0 , and $\omega(z)$ are determined. What is important, however, is the relationship between the position of the razor blade and the voltage reading on the oscilloscope. After mounting the valve to the translation stage, the displacement of the strip can be quantified by recording the maximum and minimum voltage readings during the strip's motion, finding these voltages on the error function curve, and reading off the difference between the two corresponding positions (see Figure 4.2). Before making this measurement, the valve is moved into a position where the voltage reading is in the middle of the range seen on the error function curve, ensuring that the strip motion remains within the linear regime of the curve.

In an effort to determine the optimal parameters, data for the valve motion was taken in a variety of scenarios. The parameters that were explored in detail were the pulse length and strip material. A RIGOL oscilloscope with a USB port was used to take the data, which was then transferred to a computer and plotted in OriginPro. Chapter 5 contains the most interesting results from the mechanical motion test.

Although the mechanical motion test cannot be used to characterize the performance of the newest valve design, it was of paramount importance in determining the optimal strip material.

4.2 Gas Pulse

In the gas pulse test, a gas pulse produced by the valve is measured directly. The bottom face of the valve flange is connected to a vacuum chamber, while the top face is in contact with the air. A fast ion gauge is used to measure the time profile of the pulse of air molecules created by the valve. When the valve is installed in conjunction with the rest of the molecule deceleration apparatus, the gas in the gas reservoir will be held at about 850 torr, which is slightly higher than the ambient pressure (700 torr) of the air molecules used in the gas pulse test described here. However, the gas pulse test still provides valuable insight into the performance of the valve.

The experimental apparatus is seen in Figure 4.3. The testing chamber itself is a conflat

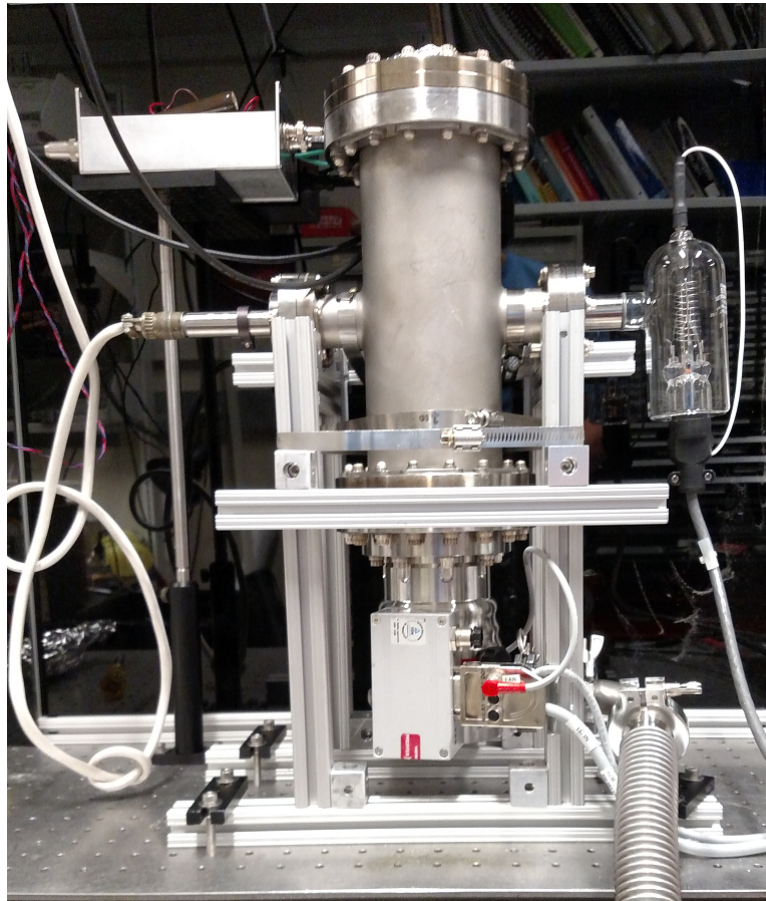


Figure 4.3: To characterize the performance of the valve, a fast ion gauge the pulse of air molecules that it creates within the testing chamber.

tee, with 6" flanges on the top and the bottom, and a 2-3/4" flanges on either side. The valve flange is attached to the top 6" flange via a 6" to 2-3/4" zero-length reducer. A turbomolecular pump is connected to the bottom 6" flange via a 6" to 4-1/2" zero length reducer. A roughing pump is connected to the turbo pump with KF bellows. The roughing pump itself is connected to a shared exhaust line within the lab. A thermocouple (TC) gauge, used to measure the pressure down to about 10^{-2} Torr, is also connected to the roughing pump. The 2-3/4" flanges protruding from either side of the testing chamber are used to attach an ionization gauge and a fast ionization gauge (FIG). The ion gauge measures the average pressure of the testing chamber once it has been pumped down to below 10^{-4} Torr (the ionization gauge cannot be used at higher pressures, or the filament could burn out). The FIG (Jordan TOF Fast Ion Gauge B-451), as its name might suggest, measures the pressure with a much greater time resolution. In other words, the fast ion gauge measures the time profile of the gas pulse produced by the valve.

The experimental set-up also includes copious amounts of electronics. The custom valve electronics, described in Chapter 2, are situated near the valve to minimize the length of the leads. The valve electronics are connected to a function generator, to supply the square wave pulse to the gate of the FETs, a ± 15 V power supply, to power the buffer amplifier, and a 20 V floating power supply, to charge the bank of capacitors. The TC gauge and the ion gauge are connected to electronics that display the pressure readings from both. The FIG is controlled by an electronic panel that allows adjustment of the filament current and voltage. A BNC cable is used to connect the output of the FIG to an oscilloscope.

Before the gas pulse produced by the valve is measured, the valve must be sealed. As mentioned in Chapter 3, the closing tension of the valve is adjusted by screwing the valve body tighter into the valve flange. However, if the valve is over-tensioned, the strip will not be able to retract fully, and the gas pulse produced will be less dense. In addition to this, there will be a greater delay between triggering the pulse and the production of the gas pulse because of the extra time it takes for the ball to decompress from the O-ring before the gas begins flowing through. The process of sealing the valve is performed as follows:

- (1) Turn on the roughing pump and ensure that the reading on the TC gauge begins to drop
- (2) Slowly screw the valve body into the valve flange until the ball makes contact with the O-ring and the pressure begins to drop noticeably
- (3) When the TC gauge reads 10^{-2} Torr or lower, turn on the turbo pump
- (4) Wait for the turbo pump to spin up to its maximum frequency (in our case, 1500 Hz)
- (5) Turn on the ionization gauge to read the pressure in the chamber
- (6) Wait a minute or two for the chamber to pump down to its minimum pressure
- (7) Slowly increase the closing tension of the valve until the pressure in the chamber drops below 10^{-6} Torr

If the pressure fails to drop low enough as the closing tension of the valve is increased, the strip should be exchanged for another one. Because the process of fabricating the strips is somewhat inconsistent, the sphericity of the Torr Seal ball can vary. A quick test can be performed check a batch of strips to find which ones seal against the O-ring the most effectively: after setting aside the valve body, the relative sealing performance of each strip is determined by placing them one by one onto the O-ring in the valve flange (the Torr Seal ball will suction onto the O-ring, holding the strip up) with the roughing pump running and watching how low the pressure of the chamber pumps down to for each.

After the optimal closing tension of the valve is found, and the chamber pumps down to below 10^{-6} Torr, the valve is ready for operation. The process of measuring the gas pulse produced by the valve is as follows:

- (1) Turn on the FIG and set the current and voltage values to the middle of the scale
- (2) Power on the ± 15 V power supply for the buffer amplifier
- (3) Power on the function generator and set it to produce a short pulse (e.g., $12.5 \mu\text{s}$, $25 \mu\text{s}$)
- (4) Making sure that the voltage is less than 10 V, turn on the floating power supply (at this point, the valve should start softly clicking as it operates)
- (5) Slowly increase the voltage of the power supply until a waveform begins to appear on the oscilloscope
- (6) Adjust the current and voltage on the FIG to get the largest pulse possible

Like in the mechanical motion test, a RIGOL oscilloscope with a USB port is used to take the data. The data is transferred to a computer, where OriginPro is used to plot and fit the data.

Chapter 5

Data and Analysis

The primary goal of the research behind this thesis was to create a new pulsed molecular beam valve capable of producing an internally cold, dense molecular beam. Ideally, the performance would be better than that of the PZT valve currently used in our lab. The two methods of measurement, the mechanical motion test and the gas pulse test, characterize the performance of the valve, allowing a direct comparison to PZT valve and other common valve types. In addition to quantifying the performance of the valve to compare to other valves, the measurements provided a systematic way of altering valve parameters and analyzing the results to find the ideal configuration of the valve.

5.1 Mechanical Motion Results

The mechanical motion test, described in Section 4.1, allows the direct measurement of the speed and displacement of the metal valve strip. Because the strip itself has to move a small amount to decompress from the O-ring before the gas begins to flow through the nozzle, the speed of the strip itself sets an upper limit on the width (duration) of the gas pulse produced. Besides establishing this limit, the mechanical motion test cannot deduce anything about the width of the gas pulse produced. The displacement of the strip is related to the density of the molecular beam produced—although the exact relationship is complicated, we can qualitatively say that a strip that displaces further will create a denser molecular beam when all other factors are held constant. Ideally, the valve strip will be able to displace far enough to reach choked flow, a regime where

the velocity of the gas reaches its limit and the flow reaches a maximum for the given pressure differential. (Up to this point, larger displacements allow more molecules to flow through at a time, resulting in a denser molecular beam.) Although the measurements of strip opening times and displacements cannot be used in any obvious way to calculate the gas pulse width or density, respectively, they still provide a useful measure of the relative performance of the valve under different operating parameters.

The mechanical motion of the strip can be divided into two distinct motions. The first is the **current-driven motion**, in which the strip moves upwards. This motion occurs during the duration of the driving pulse, while current is flowing through the strip. During this time, the Lorentz force exceeds the spring force of the strip, and the net force of the strip is upwards, causing it to accelerate upwards. The second is the **spring-driven motion**. This motion occurs once the current ceases to flow through the strip, and the net force on the strip is dictated by the spring force, causing a downwards acceleration. For the first part of the spring driven motion, the strip continues to move upwards with a decreasing velocity. The furthest position from equilibrium that the strip attains is the **strip displacement**. Once the velocity switches direction, the strip moves back towards its original position. The speed of the valve, the **opening time**, is measured as the FWHM width of the curve that describes this total motion on a displacement versus time plot.

The first parameter that was explored in depth with the mechanical motion test was the strip material and the driving-pulse length. The strip material must be lightweight, durable, springy and conductive. With these characteristics in mind, several materials were chosen to test: aluminum (Al) 6061 alloy, Beryllium Copper (BeCu), sterling silver, and titanium. The Al 6061 was taken from aluminum window blinds, with a thickness measured at 0.006". The thicknesses of the other materials was chosen to match this thickness. BeCu, also known as spring copper, is the strongest alloy of copper. Because of its high copper content, it is very conductive. Sterling silver (92.5% silver, 7.5% copper) is also very conductive. Titanium is less conductive and heavier than the other materials, but it is stronger. The mechanical motion of these different valve strips was measured under constant conditions (25 μ s pulse, 10 Hz repetition rate, and 20 V floating power supply).

The speeds of the four materials were then compared. The titanium and sterling silver strips were immediately discounted because the opening time (FWHM) was in the hundreds of microseconds. The performances of the Al 6061 and the BeCu were far better. The results of the mechanical motion for these two materials is seen in Figure 5.1 (the voltage versus time plots extracted from the oscilloscope are converted to displacement versus time plots using the method described in Section 4.1).

Although the the displacements of the strips are similar (a change in voltage from 1.5 V to 1.0 V is equivalent to a displacement of approximately 200 μm), the response of the aluminum strip is significantly faster. Aluminum is chosen as the valve strip material for this reason. Although the Al 6061 was used at first because of its availability, there are countless other alloys of aluminum. The Nijmegen Pulsed Valve uses valve strip that is 1-3% silicon alloyed in aluminum [19]. The closest commercially available aluminum alloy is Al 4043, 5% silicon alloyed in aluminum. This alloy is commonly found in welding rods, which can be rolled out to make strips of the proper thickness (see Section 3.2.2.4). The results of the mechanical motion test to compare the Al 6061 and 4043 alloys is seen in Figure 5.2.

Again, the difference is significant. The opening times of the Al 6061 and Al 4043 strips are, respectively, approximately 150 μs and 100 μs FWHM. The displacements are similar, about 200 μm . The negatively sloping part of the curve corresponds to when the Lorentz force is moving the strip upwards. During this stage, the motion of the strip is primarily dictated by the mass of the material ($F = ma$). Because the two strip types are mostly composed of aluminum, their mass (and thus their motion) is similar. The positively sloping part of the curve corresponds to when the strip is springing back downwards by itself. It appears that the Al 4043 is springier than the Al 6061, allowing it to close at about twice the rate. Aluminum 4043 is lightweight, conductive, and springy, making it an ideal choice for the strip material.

Another parameter of interest is the length of the pulse that drives the valve electronics. Intuitively, one would expect a longer pulse length to force the strip to displace farther and remain open for a longer time. Using the Al 4043 strip, this test was performed for three different driving

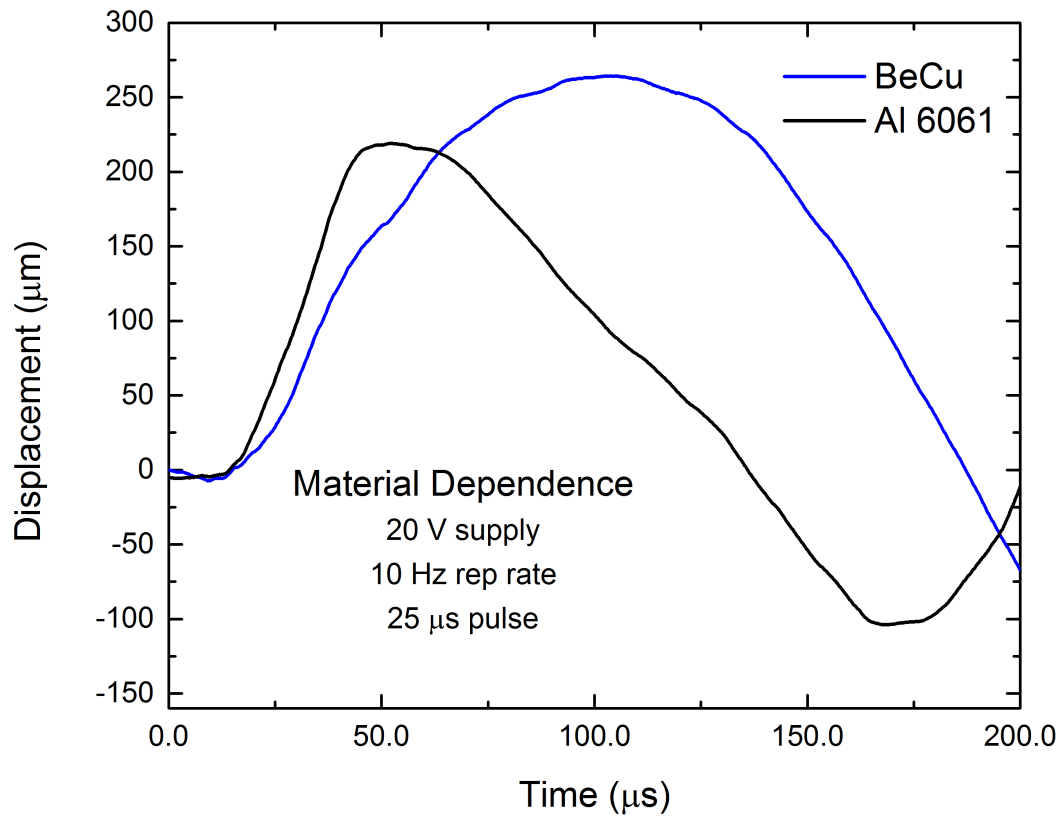


Figure 5.1: Shown here are the results for the mechanical motion of two different strip materials: Al 6061 and BeCu. The output of the photodiode connects to a transimpedance amplifier, which connects to an oscilloscope. A voltage versus time plot is extracted from the oscilloscope; the voltage reading is approximately related to the position of the strip because the strip's motion remains within the linear regime of the error function curve. The voltage versus time plot is converted to the displacement versus time plot seen here, where zero displacement is defined as the resting position of the strip.

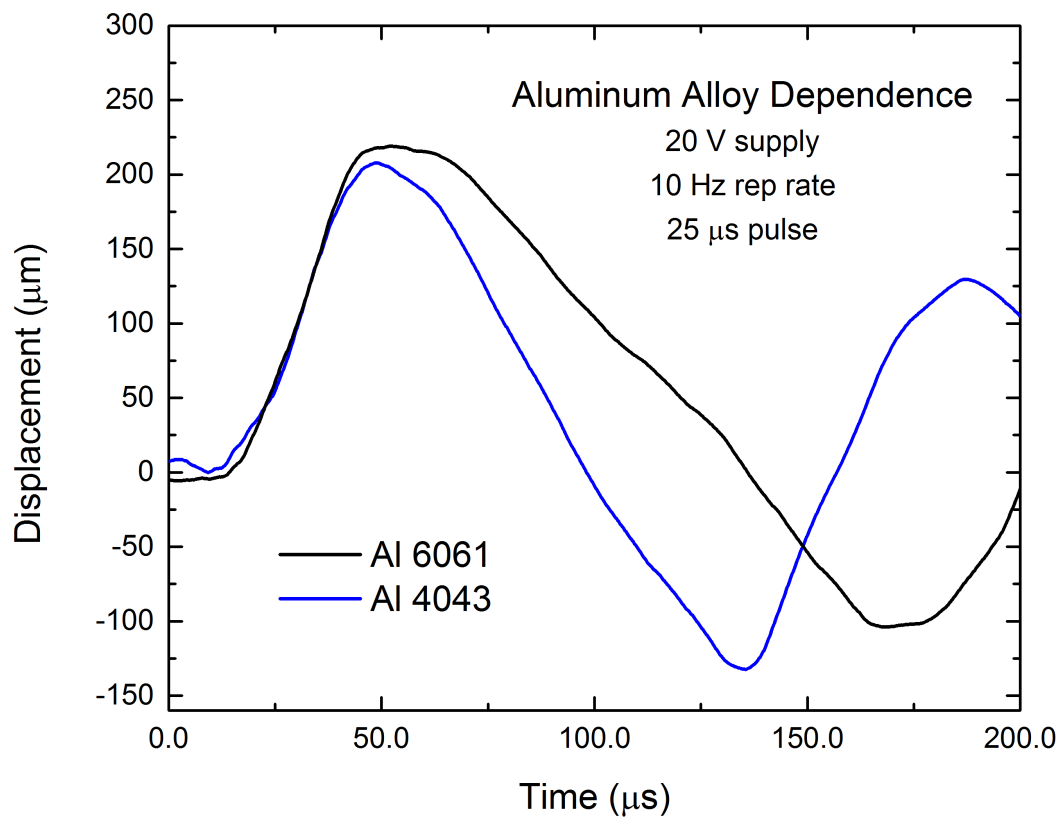


Figure 5.2: Shown here are the results for the mechanical motion of two different aluminum alloys: Al 6061 and Al 4043.

pulse lengths (12.5 μs , 16.7 μs , and 25 μs), seen in Figure 5.3.

The strip generally behaves as expected. The current-driven motion occurs during the duration of the driving pulse, resulting in a net upwards force. Mathematically, this corresponds to the region of the curve with negative concavity (the second derivative of position with respect to time is acceleration). The spring-driven motion occurs once the driving pulse is turned off. The length of time that this motion takes is longer than the length of the driving pulse because the strip must first slow its upwards movement before springing back down. Because of this, the total opening time (in this case, not FWHM) is more than twice the length of the driving pulse. Clearly, the resonant frequency of the strip material used imposes a limit on how much decreasing the length of the driving pulse can decrease the length of the opening time. However, the speeds achieved here with the aluminum 4043 strip are still $< 100 \mu\text{s}$ FWHM. This is a suitable starting point to begin measuring the gas pulses themselves. Changing the driving pulse length offers a trade-off between speed and displacement of the valve strip (which correspond to the width and density of the gas pulse produced). The valve is versatile in this respect—the driving pulse length can be adjusted to produce, within limits, a pulsed molecular beam with the characteristics required by a specific experiment.

5.2 Gas Pulse Results

The gas pulse test, described in Section 4.2, directly measures the shape of the gas pulse produced by the valve. In this case, the “gas reservoir” is actually the ambient atmosphere, and the gas pulse produced is composed of air molecules. Still, the pressure difference between the reservoir and the vacuum chamber is similar to that in the true experimental apparatus, and the shape of the gas pulse produced is expected to be similar. The results of the gas pulse test are seen in Figure 5.4.

It is now evident that the valve can indeed produce a short duration pulse of molecules (about 50 μs FWHM). The pulse shape remains the same with each shot of the valve. So, at least when it is configured properly, the valve has good shot-to-shot stability. However, the valve is quite fragile.

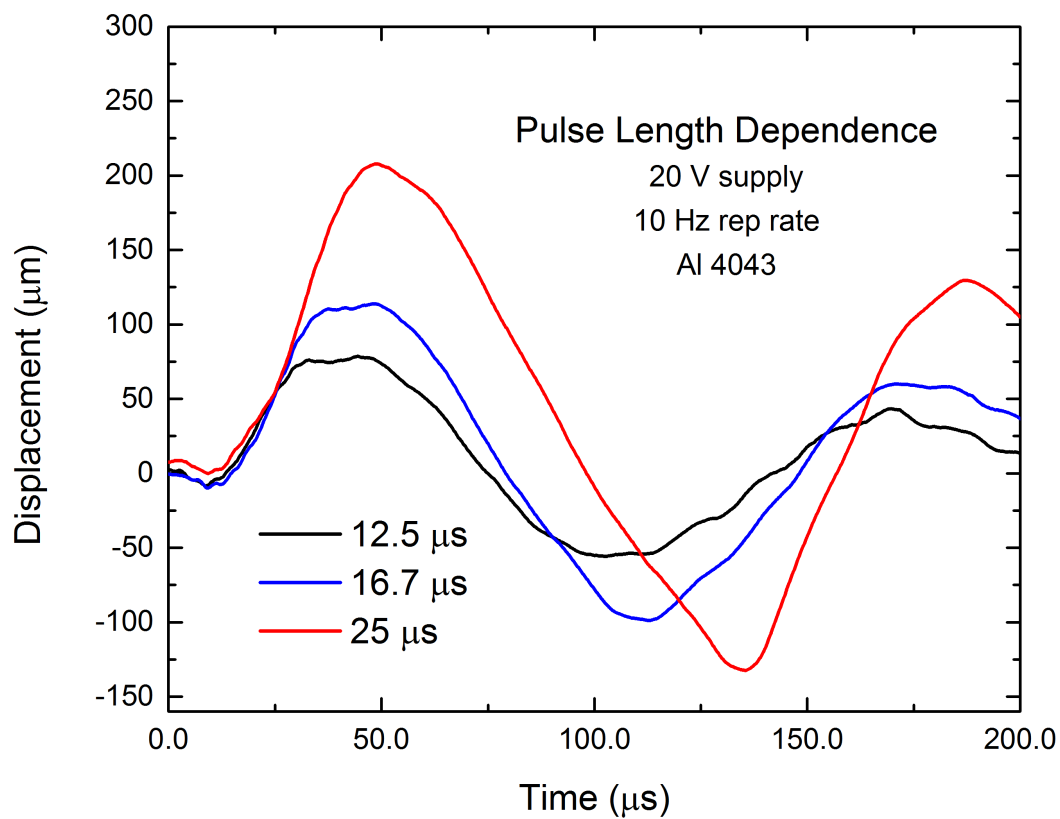


Figure 5.3: Shown here are the results for the mechanical motion of an aluminum 4043 alloy strip driven by three different pulse lengths. The current pulse is sent through the strip starting at $t = 0$.

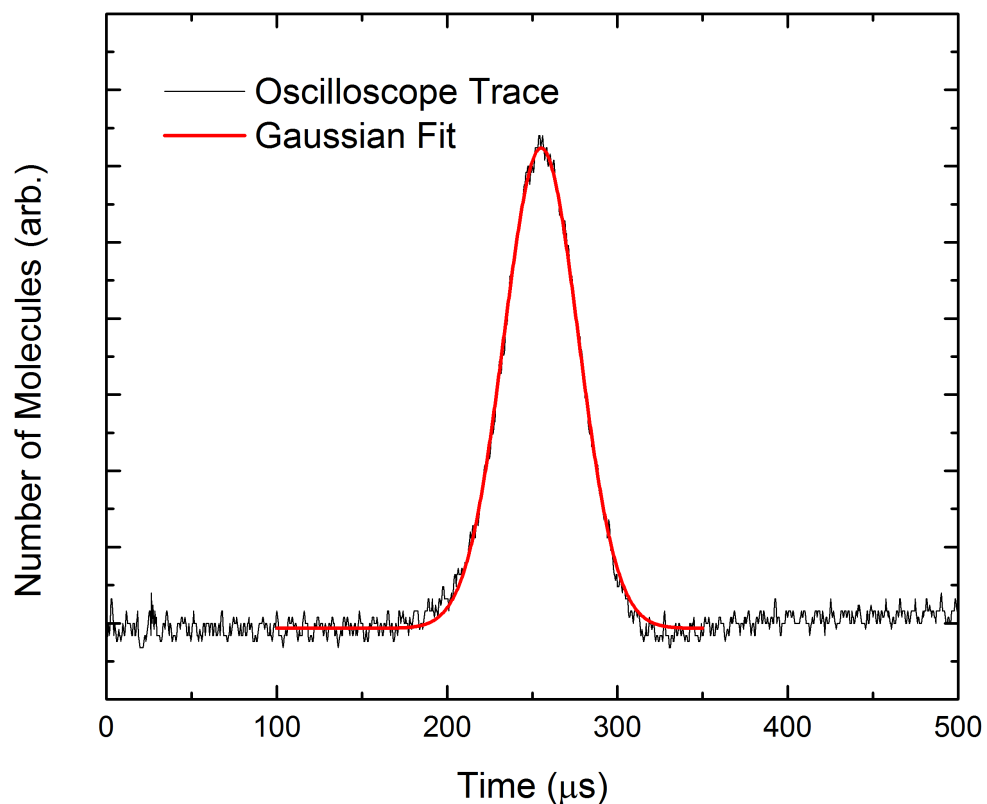


Figure 5.4: In the gas pulse test, a fast ionization gauge is used to directly measure the shape of a gas pulse produced by the valve. Because the FIG is not calibrated, the density (number of molecules per unit time) of the pulse cannot be calculated. However, the results of the test show the pulse width and the overall shape. The result is a nearly Gaussian curve with a FWHM width of approximately $50 \mu\text{s}$. The driving pulse, triggered at $t = 0$, is a $16.7 \mu\text{s}$ pulse at a 1 Hz repetition rate. The floating power supply voltage is 14 V. Note the delay between the trigger of the driving pulse and the emergence of the gas pulse. This is mostly caused by the transit time to the filament of the FIG, which is about 15 cm downstream from the valve nozzle.

Overtightening the closing tension runs the risk of bending the strip out of shape, and the valve will be unable to seal effectively.

5.3 Conclusions and Future Work

The measurements indicated that the valve can indeed produce a stable, short duration pulse of molecules. The pulse width is approximately $50 \mu\text{s}$ FWHM, which is a factor of two faster than the $100 \mu\text{s}$ pulse produced by the PZT valve currently in use of our lab. The pulse width is similar to the $60 \mu\text{s}$ FWHM achieved by the Jordan Valve and wider than the $20 \mu\text{s}$ FWHM pulses produced by the Even-Lavie Valve.

Although the valve has succeeded in creating a short duration gas pulse, the density of the pulse is less clear. According to the measurements of the mechanical motion test, the valve strip displaces by about $200 \mu\text{m}$ with driving pulses of $25 \mu\text{s}$. Again, this is a factor of two better than the $100 \mu\text{m}$ displacement of the PZT valve used in our lab. However, the mechanical motion test was performed on an earlier prototype of the valve that lacked a sealing mechanism. It is entirely possible that the closing tension between the ball and the O-ring in the current valve prototype reduced the maximum opening displacement. For this reason, the mechanical motion test cannot serve as a direct point of comparison between the new valve and the PZT valve (although, to reiterate, it was invaluable to compare the relative performance of the valve in different configurations). A possible avenue of future research would be to adapt the PZT valve to work with the same testing chamber used to perform the gas pulse test on the valve. This way, the gas pulses produced by these two valves could be compared directly.

In addition to this, there is still work to be done to adapt the valve to run in tandem with the molecule deceleration experiment. In order to do this, a valve housing must be developed (see Section 3.1.1) that seals against the back face of the valve flange and creates an isolated gas reservoir. The PZT valve currently used in our lab is mounted entirely within vacuum. A gas line and electrical connections are routed through to it from the outside of the vacuum chamber. Ideally, the new valve would be able to be installed in a similar manner, with a gas line and the two leads

from the valve circuit leading to within the valve housing. At this point, the valve could be tested in conjunction with the Stark decelerator to further probe the characteristics of the molecular beam it produces (a colder beam could be trapped more efficiently).

Another direction to explore in the future is in regards to the reliability of the valve. Although the valve succeeded in creating a short duration gas pulse with excellent shot-to-shot stability, these results are not easy to obtain. Sealing the valve body against the valve flange is a tricky process that involves turning the valve body by small increments and carefully monitoring the pressure changes read by the ionization gauge. Overtensioning the valve runs the risk of deforming the fragile aluminum strip. This process must be streamlined before the valve can be used effectively in the entire experimental apparatus—there is no way to fine tune the closing tension once the valve housing has been installed and the entire assembly has been placed in vacuum.

Nevertheless, the research behind this thesis has succeeded in designing, constructing, and characterizing a new pulsed molecular beam valve based on the design of the Nijmegen Pulsed Valve. After countless prototypes, the valve and its associated electronics have emerged in their current form. With a modest engineering skillset and a little bit of motivation, a low cost pulsed valve can be created.

Bibliography

- [1] M. N. R. Ashfold, R. N. Dixon, R. J. Stickland, and C. M. Western. 2+1 MPI spectroscopy of B 1e" state NH₃ and ND₃: rotational analysis of the origin bands. Chemical Physics Letters, 138(2):201–208, July 1987.
- [2] Hendrick L. Bethlem, Giel Berden, and Gerard Meijer. Decelerating Neutral Dipolar Molecules. Physical Review Letters, 83(8):1558–1561, August 1999.
- [3] Lincoln D. Carr, David DeMille, Roman V. Krems, and Jun Ye. Cold and ultracold molecules: science, technology and applications. New Journal of Physics, 11(5):055049, 2009.
- [4] Wolfgang Christen and Klaus Rademann. Cooling and slowing in high-pressure jet expansions. Physical Review A, 77(1):012702, January 2008.
- [5] J. Doyle, B. Friedrich, R. V. Krems, and F. Masnou-Seeuws. Editorial: Quo vadis, cold molecules? The European Physical Journal D - Atomic, Molecular, Optical and Plasma Physics, 31(2):149–164, November 2004.
- [6] U. Even. The Even-Lavie valve as a source for high intensity supersonic beam. EPJ Techniques and Instrumentation, 2(1), December 2015.
- [7] W. R. Gentry and C. F. Giese. Ten-microsecond pulsed molecular beam source and a fast ionization detector. The Review of Scientific Instruments, 49(5):595, May 1978.
- [8] K&J Magnetics. K&J Magnetics Blog.
- [9] L.P. Parazzoli, N.J. Fitch, P.S. Zuchowski, and H.J. Lewandowski. Large Effects of Electric Fields on Atom-Molecule Collisions at Millikelvin Temperatures. Physical Review Letters, 106(19), 2011.
- [10] Mean free path, January 2016. Page Version ID: 702246733.
- [11] Michael D. Morse. 2. Supersonic Beam Sources. In F. B. Dunning and Randall G. Hulet, editor, Experimental Methods in the Physical Sciences, volume 29, Part B of Atomic, Molecular, and Optical Physics: Atoms and Molecules, pages 21–47. Academic Press, 1996.
- [12] NIOSH. Worker deaths by electrocution.
- [13] N.J. Fitch. Traveling-Wave Stark-Decelerated Molecular Beams for Cold Collision Experiments. PhD thesis, University of Colorado, Boulder, 2013.

- [14] Andreas Osterwalder, Samuel A. Meek, Georg Hammer, Henrik Haak, and Gerard Meijer. Deceleration of neutral molecules in macroscopic traveling traps. Physical Review A, 81(5):051401, May 2010.
- [15] D. Proch and T. Trickl. A high-intensity multi-purpose piezoelectric pulsed molecular beam source. Review of Scientific Instruments, 60:713–716, April 1989.
- [16] R.M. Jordan. PSV Pulsed Supersonic Valve C-211.
- [17] Katherine L. Saenger. Pulsed molecular beams: A lower limit on pulse duration for fully developed supersonic expansions. The Journal of Chemical Physics, 75(5):2467–2469, September 1981.
- [18] Umea University. Characterization of a Gaussian shaped laser beam.
- [19] B. Yan, P. F. H. Claus, B. G. M. van Oorschot, L. Gerritsen, A. T. J. B. Eppink, S. Y. T. van de Meerakker, and D. H. Parker. A new high intensity and short-pulse molecular beam valve. Review of Scientific Instruments, 84(2):023102, February 2013.

